**Enhanced Mechanical Properties of Aliphatic Polyester Thermoplastic Elastomers through Star Block Architectures** 

Stephanie Liffland and Marc A. Hillmyer\*

Department of Chemistry, University of Minnesota, Minneapolis, MN 55455-0431

# **TOC Graphic**

## **Abstract**

A series of sustainable aliphatic polyester thermoplastic elastomers (APTPEs) consisting of multiarm star polymers with arms of poly(L-lactide)-*b*-poly(γ-methyl-ε-caprolactone), were investigated and compared to analogous linear poly(L-lactide)-*b*-poly(γ-methyl-ε-caprolactone)*b*-poly(L-lactide) triblock polymers. Linear analogues with comparable arm molar mass and comparable overall molar mass were synthesized to distinguish architectural and molar mass effects. Overall, the star block polymers significantly outperformed their linear analogues with respect to ultimate tensile strength and tensile toughness, exhibiting more pronounced strain hardening than corresponding linear APTPEs. The stars exhibited high ultimate tensile strengths (~33 MPa) and large elongations at break (~1400 %), outperforming commercially relevant, petroleum-derived, and non-degradable styrenic TPEs. The star polymers also exhibited superior recovery characteristics during cyclic strain cycles and reduced stress relaxation compared to the

linear APTPEs, highlighting the impact of architecture on improved TPE mechanical properties.

Dynamic mechanical thermal analysis suggests that the star architecture increases the usage

temperature range does not negatively influence processability, an important feature for future

applications. Overall, this work illustrates that simple and convenient changes in the

macromolecular architecture in sustainable APTPEs results in materials with greatly enhanced

mechanical properties. A comprehensive understanding of the relationship between polymer

architecture and mechanical properties can be capitalized on to develop property-specific and

industrially relevant sustainable materials.

\*Corresponding author (e-mail: hillmyer@umn.edu)

2

## Introduction

Due to their low cost of manufacturing, versatile properties, and ability to undergo rapid (re)processing, thermoplastic elastomers (TPEs) are used in applications ranging from adhesives to personal care products. The most common architecture for TPEs is that of a linear ABA triblock polymer, where the A end blocks consist of a hard (high glass transition ( $T_g$ ) or high melting temperature ( $T_m$ )) polymer, while the B midblock is a soft (low  $T_g$ ) and rubbery polymer. Characterized by their high tensile strength, tunable modulus, and efficient elastic recovery, TPEs behave similarly to chemically crosslinked elastomers at their usage temperatures. These elastomeric properties are a direct result of microphase separation, where the A blocks, which make up the minority component, form discrete hard domains within a matrix of the rubbery B component; the hard domains act as anchors that physically crosslink the rubbery midblocks. Additionally, any trapped entanglements in the rubbery domain act as effective cross-links, further enhancing elastomeric behavior and material strength.

The majority of commercial TPEs are petroleum-derived, typically containing hard polystyrene (PS) end blocks and either a polybutadiene (PB) or polyisoprene (PI) midblock.  $^{1,3,4}$  Significant research has been devoted to the development of sustainable alternatives to petrochemical-based TPEs that improve upon both renewability and degradability.  $^{5-14}$  Previous aliphatic polyester TPEs (APTPEs) of poly(L-lactide)-b-poly( $\gamma$ -methyl- $\epsilon$ -caprolactone)-b-poly(L-lactide) (PLLA-P $\gamma$ MCL-PLLA) reported by our group exhibited ultimate tensile strengths ( $\sigma$ B) and elongations at break ( $\epsilon$ B) comparable to commercial incumbents.  $^{1,9}$  However, while these materials showed promising stress-strain behavior, they had an undesirable stress relaxation behavior in the strained state at moderate temperatures.

Stress relaxation can be caused by chain pullout, where the A end-blocks are forced from the hard domains into the rubbery B phase upon deformation. The extent of this chain pullout is temperature-dependent and increases significantly as the system approaches the glass transition temperature of the hard blocks  $(T_{g,A})$ . Chain pullout, paired with permanent deformation of the hard domains under sufficient applied stress, leads to the observed stress relaxation as well as undesirable creep behavior, which can in turn result in increased permanent set (higher residual strains). Such aspects of TPEs can impact long-term material performance.

Attempts to mitigate these deleterious effects in TPEs and further improve mechanical properties have included the introduction of composite hard domains (i.e., containing both glassy and crystalline blocks), <sup>21,22</sup> chain extension to generate –(AB)<sub>n</sub>– multiblock polymers, <sup>6,23–25</sup> end-group functionalization with supramolecular, self-associating moieties (*e.g.*, hydrogen bonding units), and the use of nonlinear block architectures. <sup>26,27</sup> In particular, (AB)<sub>n</sub> star block polymers, where *n* is the number of arms, have received significant attention due to their simple, well-defined architectures and advantageous rheological properties (i.e., relatively low melt viscosities). <sup>28,29</sup> Star block TPEs have been shown to outperform their linear analogues in terms of ultimate tensile strength and display a reduced sensitivity to diblock contamination; <sup>29–34</sup> however, this is often accompanied by a decrease in the elongation at break. <sup>28–31</sup> The improved mechanical properties in star TPEs are thought to result from the core of the star, which acts to more effectively distribute applied stresses during deformation. <sup>28,29</sup>

While the implementation of star architectures in styrenic TPEs has been well-studied,<sup>26–33</sup> reports of aliphatic polyester star block TPEs are comparatively rare.<sup>35–38</sup> In 2000, Joziasse *et al.*<sup>35</sup> detailed the synthesis and characterization of star block polymers of poly(trimethylene carbonate-*co*-(ε-caprolactone)) from a variety of initiators. Further reaction of the rubbery cores with mixtures of D,L-lactide and glycolide provided star block polymers with hard block wt % of

67–83%. However, the composition of these polymers ( $f_A > 0.50$ ) resulted in materials that displayed yielding and ductile tensile behavior, characteristic of rubber modified plastics with enhanced toughening<sup>39</sup> rather than the elastomeric behavior of TPEs. Kong *et al.*<sup>37</sup> reported 4-arm stars comprised of poly(caprolactone-*co*-L-lactide) cores and poly(L-lactide) end blocks. Cyclic strain experiments showed that the star polymers with 22 wt % PLLA recovered >10% more (lower residual strains) than linear analogues when extended to 150% strain.<sup>40</sup> However, despite the improvement in recovery, the star polymers displayed fairly low ultimate tensile strengths (~4 MPa) and moderate elongations at break (300–600%). Recently, Lee *et al.*<sup>38</sup> synthesized and characterized a series of multi-arm star block polymers of poly( $\epsilon$ -decalactone) and poly(L-lactide) with constant molar mass (180 kg mol<sup>-1</sup>) and volume fraction PLLA ( $f_{PLLA} = 0.27$ ). They found that at a fixed molar mass and block ratio, material tensile properties were highly dependent on the number of arms (n). The ultimate tensile strength was found to increase from 8 to 15 MPa as the arm functionality was increased from 2 to 6; however, the reported elongations at break decreased from about 1800% to 1000%.

In this work, we seek to systematically study the effect of arm number and molar mass on the mechanical properties of APTPEs of PγMCL and PLLA. We posit that the implementation of a star architecture will both improve mechanical properties and mitigate stress relaxation through the ability of the permanent crosslink from the core of the star to maintain elastically effective connections between the rubbery and hard domains even when chain pullout occurs.<sup>31</sup> We report the convenient synthesis and characterization of a series of sustainable (poly(L-Lactide)-*b*-poly(γ-methyl-ε-caprolactone))<sub>n</sub>, (LLM)<sub>n</sub>, multi-arm star block polymers with rubbery inner blocks and semicrystalline and glassy hard blocks by a one-pot, two-step synthesis methodology. We discuss the impact of catalyst selection on the mechanical properties of the APTPEs and demonstrate the

advantages of the star architecture in these materials. We then investigate the impact of increasing arm number on thermal, rheological, tensile, and stress relaxation behavior while holding the arm molar mass constant. To distinguish the impact of architecture from molar mass effects, the mechanical properties of the star APTPEs were compared to those of linear analogues at similar overall molar masses, as our previous work has shown that high-molar-mass TPEs are mechanically superior to their low-molar-mass variants. Lastly, we study the effect of increasing star functionality on systems with constant, moderate molar mass to explore advantages of the star architecture in the lower-molar-mass limit.

## **Experimental Summary**

Details for the synthesis and purification of the (LLM)<sub>2</sub>, (LLM)<sub>4</sub>, and (LLM)<sub>6</sub> star block APTPEs and appropriate monomers are comprehensively covered in the Supporting Information (SI). Specifics regarding the processing methodology used to prepare polymer samples for analysis by differential scanning calorimetry (DSC), small angle x-ray scattering (SAXS), size exclusion chromatography (SEC), dynamic mechanical thermal analysis (DMTA), tensile testing, and stress relaxation experiments, as well as the relevant characterization parameters and instrument details, are also included in the SI.

#### **Results and Discussion**

## **Polymer Design and Synthesis**

Our initial studies maintained a constant arm molar mass ( $M_{arm}$ ) in each of the star polymers. With respect to self-assembled phase behavior, Matsen<sup>41</sup> has argued that appropriate comparisons between star polymers with differing numbers of arms (n) require a fixed number of repeat units in each arm. With this in mind, star functionalities of 2 (the parent ABA triblock case

or 2-arm "star"), 4, and 6 were selected based on previous reports that ultimate tensile strength in star polymers reaches a plateau at around  $n \ge 5.^{28,29,31}$  Recent work from our group has suggested that the high-performance poly(L-lactide)-b-poly( $\gamma$ MCL)-b-poly(L-lactide) APTPEs can be accessed through a bulk, one-pot strategy.<sup>9,42</sup> However, that work focused on the synthesis of lower-molar-mass materials (<50 kg mol<sup>-1</sup>). We explored this approach for the synthesis of high-molar-mass (poly(L-lactide)-b-poly( $\gamma$ -methyl- $\varepsilon$ -caprolactone)) $_n$  ((LLM) $_n$ ) star block polymers.

$$\begin{array}{c} \text{BDM} & \text{PET} & \text{DPET} \\ \text{O-OH} & = & \text{HO} & \text{OH} & \text{or} & \text{HO} & \text{OOH} & \text{OH} \\ \text{OH} & \text{OH} & \text{OH} & \text{OH} & \text{OH} & \text{OH} \\ \end{array}$$

**Scheme 1.** Representative synthesis of star block thermoplastic elastomers (LLM)<sub>n.</sub> Polyol initiators used for synthesis of 2-, 4- and 6-arm stars are benzene dimethanol (BDM), pentaerythritol (PET), and dipentaerythritol (DPET), respectively. The catalysts indicated are 1,8-diazabicyclo[5.4.0]undec-7-ene (DBU) and tin(II) octoate (Sn(Oct)<sub>2</sub>).

We first synthesized a series of hydroxy-terminated P $\gamma$ MCL star polymers with varying numbers of arms by Sn(Oct)<sub>2</sub>-catalyzed ring-opening transesterification polymerization (ROTEP) in the melt using an appropriate initiator (Scheme 1): 1,4-benzene dimethanol (BDM) for n = 2; pentaerythritol (PET) for n = 4; and dipentaerythritol (DPET) for n = 6. Conversion was monitored by <sup>1</sup>H NMR spectroscopy, and the reactions were stopped at < 90% conversion to avoid increases in molar mass dispersity due to any intermolecular transesterification at high conversions.<sup>9,43</sup> At that point, L-lactide, CH<sub>2</sub>Cl<sub>2</sub>, and 1,8-diazabicyclo[5.4.0]undec-7-ene (DBU) (2 mol % to L-

lactide), were then added directly to the same reaction vessel under inert atmosphere. Although DBU is an effective catalyst for the ROTEP of lactide, it is not for the ROTEP of caprolactone without the addition of a thiourea co-catalyst to simultaneously activate the monomer. <sup>44</sup> This, paired with the negligible catalytic activity of Sn(Oct)2 at room temperature, <sup>45</sup> makes this catalytic system a judicious choice for polymerization of L-lactide in the presence of any residual γMCL monomer. Evidence for this approach facilitating the orthogonal polymerization of L-lactide in the presence of residual γMCL is given in the Supporting Information (Figure S1). The room temperature, organocatalyzed ROTEP of L-lactide using hydroxy-telechelic PγMCL as a macroinitiator was monitored over time by taking aliquots of the polymerization mixture for analysis by <sup>1</sup>H NMR spectroscopy. The reaction reached approximately 95% conversion of L-lactide after 40 min and near quantitative conversion after 75 min (Figure S2). A summary of the block polymers is given in Table 1.

Table 1. Summary of the star block polymers

sample ID $(M_{n,total},f_{PLLA})$	$M_{ m n,arm,P\gamma MCL}^{a} ( m kg/mol)$	M <sub>n,arm,PLLA</sub> a (kg/mol)	M <sub>n,arm,total</sub> a (kg/mol)	$M_{ m n,total}^{a} ( m kg/mol)$	$f_{ m PLLA}^b$	а	$T_{g,}$ $P_{\gamma}MCL^{d}$ (°C)	$T_{g,}$ PLLA $^d$ (°C)	$T_{\rm m,}$ PLLA <sup>e</sup> (°C)	$d^f$ (nm)
(LLM) <sub>2</sub> (67, 0.17)	26.5	6.7	33.2	67	0.17	1.31	-59	31	145	30
$(LLM)_2$ (69, 0.22)	26.6	9.0	35.6	69	0.22	1.27	-58	46	142	26
(LLM) <sub>2</sub> (149, 0.20)	57.4	17.2	74.6	149	0.20	1.53	-59	45	141	38
(LLM) <sub>2</sub> (197, 0.20)	75.8	22.9	98.7	197	0.20	1.39	-59	51	141	45
(LLM) <sub>4</sub> (70, 0.17)	13.9	3.5	17.6	70	0.17	1.22	-58	26	139	20
(LLM) <sub>4</sub> (74, 0.22)	13.9	4.6	18.5	74	0.22	1.21	-57	32	141	22
(LLM) <sub>4</sub> (138, 0.17)	27.6	6.8	34.4	138	0.17	1.53	-58	38	144	26
(LLM) <sub>4</sub> (147, 0.22)	27.6	9.1	36.7	147	0.22	1.42	-59	36	145	32
(LLM) <sub>6</sub> (68, 0.17)	9.1	2.2	11.3	68	0.17	1.14	-55	21	92, 128	18
$(LLM)_6$ (73, 0.22)	9.1	3.0	12.1	73	0.22	1.18	-56	22	135	18
$(LLM)_6$ (196, 0.17)	26.5	6.4	32.8	196	0.17	1.36	-59	35	142	27
(LLM) <sub>6</sub> (214, 0.22)	26.5	9.2	35.7	214	0.22	1.54	-58	46	143	33

<sup>&</sup>lt;sup>a</sup> Estimated by <sup>1</sup>H NMR spectroscopy using end-group analysis. <sup>b</sup> Calculated using  $\rho_{PLLA} = 1.25$  g cm<sup>-3</sup> and  $\rho_{P\gamma MCL} = 1.037$  g cm<sup>-3</sup> at 25 °C. <sup>c</sup> SEC in THF with MALLS. <sup>d</sup> Second heat in DSC heating at 10 °C min<sup>-1</sup>. <sup>e</sup> Taken as the peak of melting endotherm on second heating cycle at 10 °C min<sup>-1</sup> in a DSC. <sup>f</sup> Domain size determined from room temperature SAXS patterns using  $d = q*/2\pi$ .

SEC traces of the (LLM)<sub>n</sub> polymers show a clear increase in the molar mass of the star block polymers from their parent ( $P\gamma MCL$ )<sub>n</sub> cores (representative data is shown in Figure 1). Slight low-molar-mass tailing in the traces for the 4- and 6-arm stars is apparent, and this may be due to incomplete initiation of all hydroxyl groups at the core in a small fraction of the stars, which has been observed in previously reported star polymer systems, <sup>46</sup> or this may potentially be due to the

formation macrocycles from intramolecular transesterification.  $^{47,48}$  Further analysis of the P $\gamma$ MCL macroinitiators can be found in the Supporting Information (Figure S4). The successful growth of PLLA from the  $\gamma$ MCL cores is supported by  $^{1}$ H NMR spectroscopy and the chemical shift of the end-group resonances from  $\sim$ 3.7 ppm to  $\sim$ 4.4 ppm after initiation (Figure S5). This one-pot synthetic methodology yields the (LLM) $_n$  stars with control over molar mass and arm number through the choice of macroinitiator without the need for purification between polymerization steps.

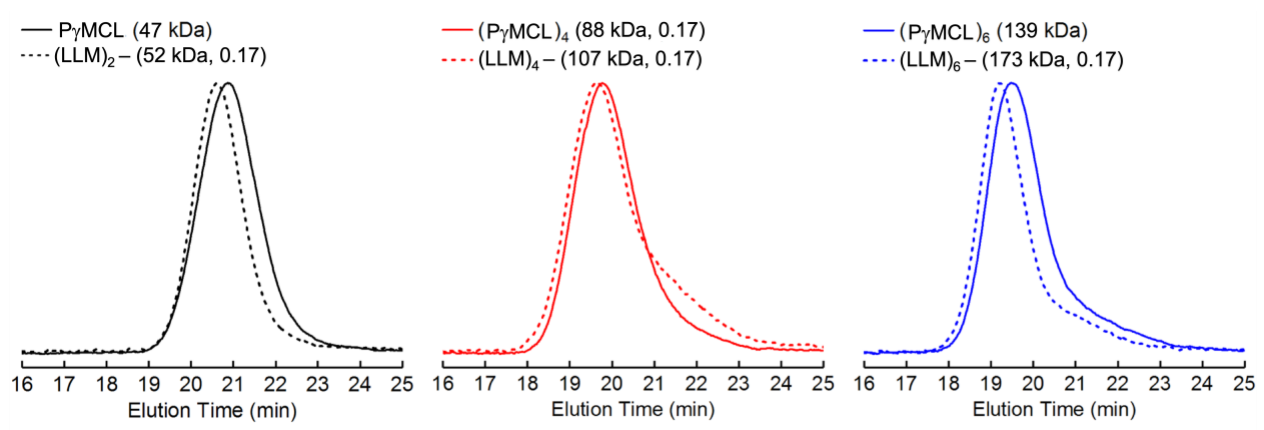


**Figure 1.** Overlay of tetrahydrofuran SEC traces for star block polymers (LLM)<sub>n</sub> (dashed) with n = 2 (left, black), 4 (middle, red), and 6 (right, blue) arms from  $(P\gamma MCL)_n$  (solid).

The star polymers exhibited two glass transition temperatures by differential scanning calorimetry (DSC), one for P $\gamma$ MCL at -59 °C and a second, broader transition ranging from 30–50 °C for the PLLA blocks depending on the specific sample, as well as a melting endotherm at approximately 143 °C for the PLLA domains (Table 1). The observed melting temperature ( $T_m$ ) for PLLA is depressed from that of high-molar-mass homopolymer ( $T_m \approx 165-175$  °C), suggesting formation of smaller PLLA crystallites. This is likely a result of the low molar mass of the PLLA blocks and the rapid cooling and vitrification of the microphase separated (see below) polymer

melt that occurs during material processing. <sup>10</sup> The suppression of PLLA crystallization is further supported by the low degrees of crystallinity ( $\phi_c = 0.08-0.18$ ) observed in the star block polymers upon the first heating cycle (Table 2).

# **Effect of Catalyst**

The DBU-catalyzed star polymers were then compared to the materials synthesized with Sn(Oct)<sub>2</sub> to investigate the effect of catalyst choice on mechanical properties of the APTPEs. Unlike the one-pot method described above, the use of Sn(Oct)<sub>2</sub> for the ROTEP of L-lactide from the (PγMCL)<sub>n</sub> macroinitiator requires the purification of the (PγMCL)<sub>n</sub> as, unlike DBU, it is not an orthogonal catalyst for the γMCL monomer. SEC traces for the Sn(Oct)<sub>2</sub>-catalyzed star TPEs indicate clear growth of the polymer without low-molar-mass tailing (Figure S8), suggesting more effective initiation from all terminal hydroxyl groups. However, a small, secondary low-molar-mass peak can be seen in the SEC traces that is not present in the DBU-catalyzed materials. This low-molar-mass impurity may be PLLA homopolymer chains initiated by adventitious water or trace hydroxyl impurities present in the polymerization mixture. <sup>45,47</sup>

The polymers were melt-pressed at 180 °C and then rapidly quenched, yielding transparent and colorless films in both cases. The films were then cut into dog bone shapes and the samples were left to age at room temperature for a minimum of 24 h before being tested under uniaxial extension at a rate of 50 mm min<sup>-1</sup> until failure. Representative stress strain curves for the samples can be seen in Figure 2. Each of the samples exhibited the expected low Young's modulus and large elongations at break typical of elastomeric behavior, as well as the strain-hardening that results in high ultimate tensile strengths. The 2-arm "star" polymers (linear triblocks) synthesized with Sn(Oct)<sub>2</sub> displayed an average ultimate tensile strength of ~21 MPa, almost double that of the

DBU-catalyzed materials at ~12 MPa. While the ultimate tensile strength of the Sn-catalyzed TPE is significantly higher than the DBU analogue, the elongation at break is lower by over 500%. The lower ultimate tensile strength and increased strain at break of the DBU-catalyzed materials suggests that the impurities present in the sample could have significant plasticizing effect on the resulting TPEs. The increased dispersity of the DBU-catalyzed 2-arm star is likely due to the presence of incompletely initiated PγMCL core and unfunctionalized PγMCL homopolymer which can prevent the formation of well-defined physical crosslinks and lead to lowered tensile strengths (Figure S10). This effect is similar to that of PS-PI diblock impurities in styrenic SIS TPEs, where the presence of anywhere from 10–20% of low-molar-mass impurities (in the form of both PS-PI diblocks and PS homopolymer) is not uncommon (Figure S11).<sup>49</sup> Rosenbloom *et al.* have also reported that the skew of the molecular weight distribution in SIS TPEs can significantly impact mechanical properties, with increased low-molar-mass PS content resulting in decreased tensile strength.<sup>50</sup>

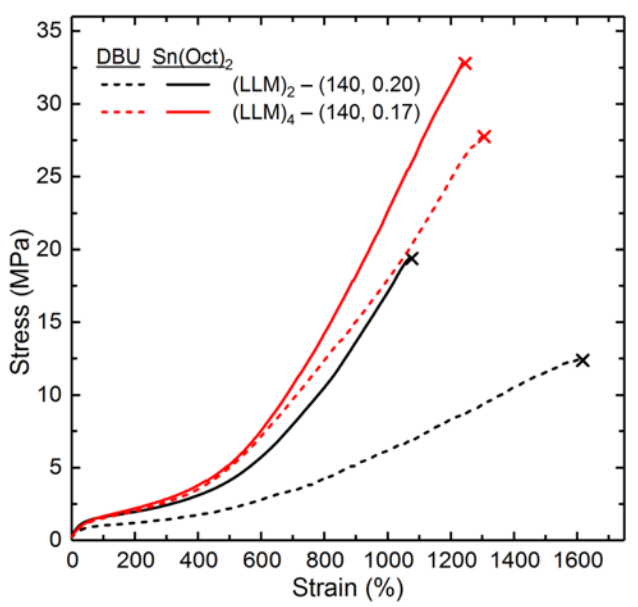


**Figure 2.** Representative stress-strain curves comparing star block polymers (LLM)<sub>n</sub> synthesized using DBU (dashed) to those of similar molar mass and composition synthesized

with  $Sn(Oct)_2$  (solid). The curves are representative from five melt-pressed dog bones pulled at 50 mm min<sup>-1</sup> to the sample break point, indicated by  $\times$ .

Interestingly, the mechanical properties of the 4-arm star polymers do not show the same sensitivity to catalyst choice as the linear APTPEs. The Sn(Oct)<sub>2</sub>-catalyzed star polymers display only a minor improvement in ultimate tensile strength (~31 MPa) when compared to DBU-catalyzed materials (~27 MPa) (Figure 2, Table 2). The insensitivity toward the putative contamination in star block polymers has been attributed to a combination of factors. These include the ability of the core of the star to more evenly distribute applied stresses to the hard domains, a larger number of hard domains per unit volume, which leads to an increased filler effect,<sup>51</sup> and improved phase separation due to more ordered and uniform hard domains.<sup>28,29</sup> Small angle X-ray scattering (SAXS) data for the APTPEs (discussed in more depth later in the manuscript) indicates that the 4- and 6-arm star polymers display smaller domain sizes compared to their linear analogues, which agrees with this idea and further supports the tensile data. These data showcase that the star polymers are more mechanically robust and "resistant" to block impurities than their linear counterparts, making them a better choice for potential applications.

The above experiments demonstrated that we were able to synthesize star block polymers with control over the number of arms through a facile one-pot methodology. The choice of polymerization catalyst appears to result in different impurities being present in the samples, which can influence material mechanical performance. However, the star architecture provides the system with resistance to the impact of these impurities compared to the linear triblocks. While the Sn(Oct)<sub>2</sub>-catalyzed star polymers show a minor improvement in ultimate tensile strength, the multiple purification steps required for their synthesis could be disadvantageous. As such, we elected to use DBU over Sn(Oct)<sub>2</sub> as a catalyst for the ROTEP of L-lactide in the synthesis of these

APTPE stars. We next explored the influence of arm number on the properties of these star block APTPEs.

# Properties of (LLM)<sub>n</sub> APTPEs with constant M<sub>arm</sub>

The microphase separated morphologies of the star polymers was determined using variable-temperature SAXS (Figures 3, S18-S21) up to 180 °C. The presence of two distinct glass transitions and the dominant scattering peaks in the room temperature SAXS patterns indicate that the star polymers are microphase separated. The samples display a principal scattering peak,  $q^*$ , with a higher order shoulder at approximately  $\sqrt{3}q^*$  and a broad peak around  $\sqrt{7}q^*$ . The calculated segregation strength  $(\gamma N)$  for these materials suggests the possibility for an order disorder transition at high temperatures ( $T \ge 180$  °C) (Table S1).<sup>41</sup> However, the polymers maintain their microphase separated morphologies at elevated temperatures (Figures S20–S21), and this is further supported by dynamic mechanical thermal analysis. The absence of distinct higher-order peaks in the SAXS pattern suggests that the stars display only a modest degree of long-range ordering and makes a definitive morphological assignment challenging. However, the broad secondary peaks resemble spherical form-factor scattering, which agrees with previous results on similar aliphatic TPEs with similar volume fractions of PLLA (Figures 3, S18). Therefore, the morphology appears to be spherical or cylindrical PLLA domains with poor long-range order. The lack of long-range order may be a result of the processing conditions used to prepare the polymers, which were meltpressed at 180 °C and then rapidly quenched to avoid complications from breakout crystallization disrupting the microphase-separated morphology. 52-54

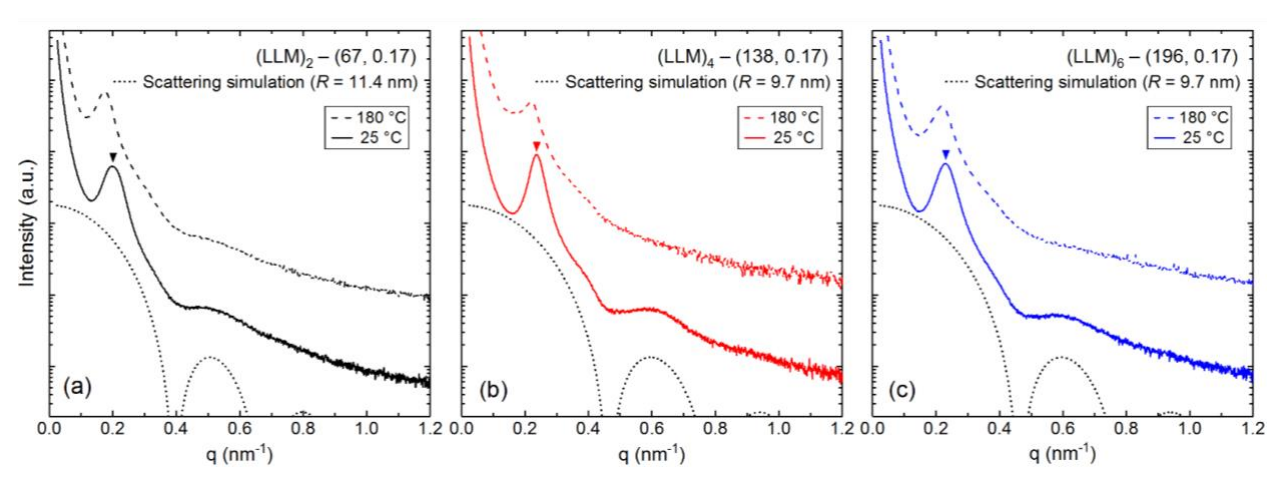
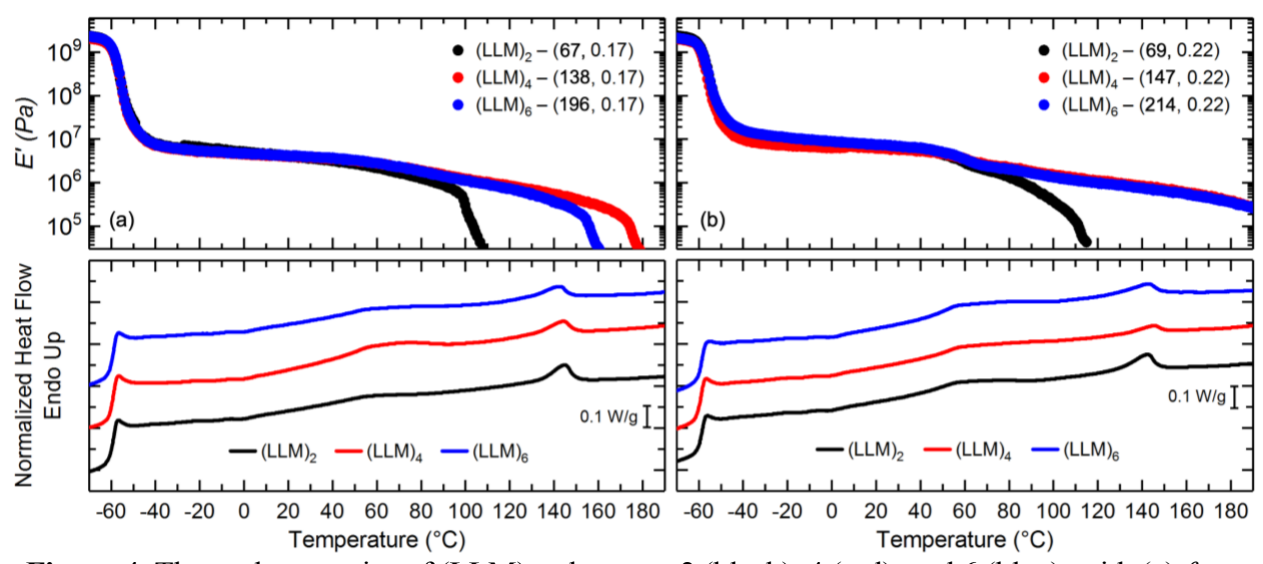


**Figure 3.** SAXS patterns of star block polymers (LLM)<sub>n</sub> at room temperature (solid) and at 180 °C (dashed) with (a) n = 2, (b) n = 4, and (c) n = 6 arms and the simulated spherical form factors (dotted). The 180 °C patterns have been shifted up for clarity (x50).

Despite its lower molar mass, the principal domain spacing of (LLM)<sub>2</sub> (67, 0.17) ( $d = 2\pi/q^*$  = 30 nm) is larger than that of both the comparable 4- and 6-arm star polymers, which have domain spacings of 26 nm and 27 nm, respectively. This result is in disagreement with previous reports from Price *et al.*<sup>55</sup> and Thomas *et al.*<sup>56</sup> who found no difference in interdomain spacing or domain diameter between (PS-PI)<sub>n</sub> star block polymers regardless of star functionality, as well as recent results from Burns *et al.*<sup>31</sup> for star polymers of (polyvinylcyclohexane-*b*-poly(ethylene-*alt*-propylene))<sub>n</sub>. However, the disparity between domain spacing of the linear triblocks and multi-arm stars was not observed in the series with  $f_{PLLA} = 0.22$ . The somewhat smaller domain sizes observed in the 4- and 6-arm stars with  $f_{PLLA} = 0.17$  may be due to restrictions on the inner PyMCL block imposed by the permanent crosslink at the core of the star, suggesting that the 4- and 6-arm star polymers possess a greater number of hard domains per unit volume than analogous linear materials.<sup>41,56–58</sup> This increase in the number of discrete hard domains may play a part in the

improved tensile properties observed in the 4- and 6-arm star polymers compared to the linear triblocks, the specifics of which are discussed later.

The moduli of compression-molded films of the star polymers in uniaxial extension were measured as a function of temperature using DMTA (Figure 4). All samples display a drop in the modulus near -57 °C due to the glass transition of PyMCL. The moduli in the rubbery plateau region for the star polymers remains constant at E'  $\approx 3.5$  MPa until approximately 50 °C where a slight decrease in the plateau modulus of the stars can begin to be observed (Figure 4), likely due to passing through the glass transition of the PLLA domains. This gradual softening of the materials persists with increasing temperature until material failure, indicated by a precipitous drop in the modulus. (LLM)<sub>2</sub> (67, 0.17) softens around 100 °C, which agrees with previous results for similar materials, while the (LLM)<sub>4</sub> (138, 0.17) and (LLM)<sub>6</sub> (196, 0.17) exhibit solid-like behavior to 175 °C and 160 °C, respectively. The increase in the usage temperature range is even more pronounced in the star polymers with higher PLLA volume fractions ( $f_{PLLA} = 0.22$ ), where the 4and 6-arm stars both display softening temperatures of over 190 °C compared to only 110 °C for the linear triblock (Figure 4). We posit that the unexpectedly high softening temperatures ( $T > T_{\rm m}$ , PLLA) observed in the 4- and 6-arm stars may be a result of the star architecture. The chemical crosslink at the core of the star may act to help maintain mechanical integrity in the ordered materials above the  $T_{\rm m}$  of PLLA when any crystallites have melted and segmental mobility of the PLLA domains is high.



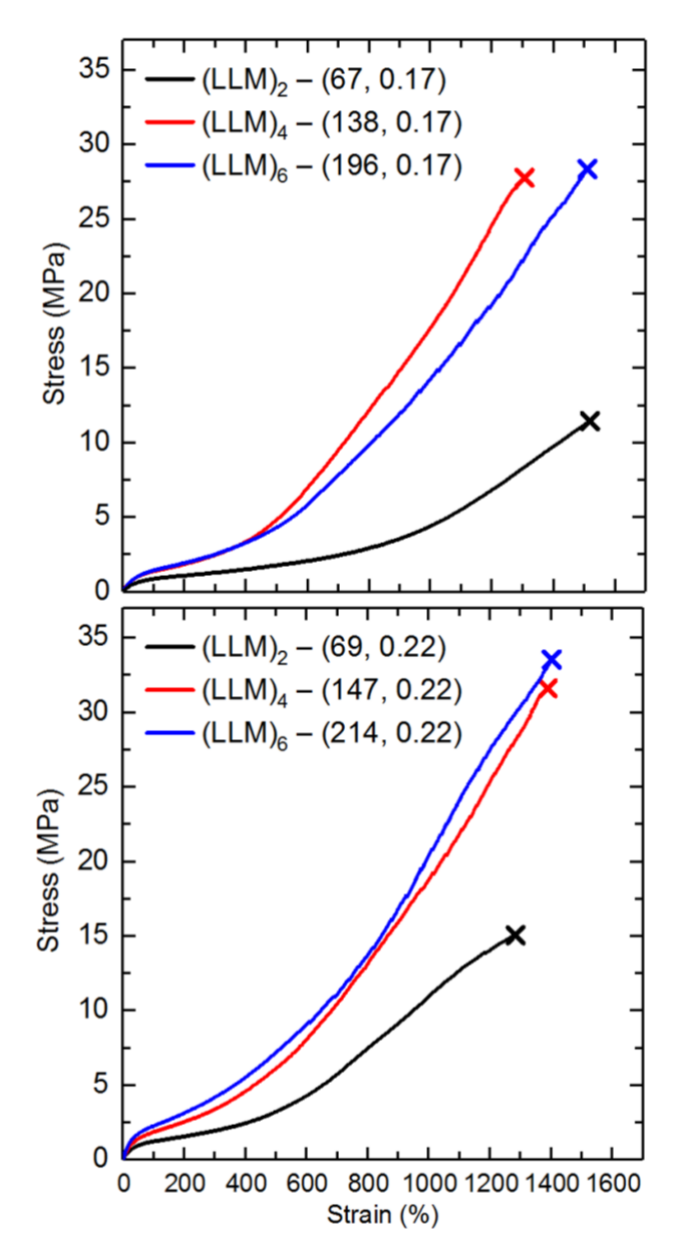
**Figure 4**. Thermal properties of (LLM)<sub>n</sub> where n = 2 (black), 4 (red), and 6 (blue), with (a)  $f_{PLLA} = 0.17$  and (b)  $f_{PLLA} = 0.22$  analyzed by DMTA in tension upon heating at 5 °C min<sup>-1</sup> (top, 1 Hz, 0.05% strain); and DSC upon heating at 10 °C min<sup>-1</sup> (bottom).

Figure 5 shows representative stress-strain curves for the star APTPEs, and average values with standard deviations for Young's modulus (E), ultimate tensile strength ( $\sigma_B$ ), elongation at break ( $\varepsilon_B$ ), and tensile toughness values are in Table 2. At small extensions ( $\varepsilon \le 50$  %) the tensile stress is expected to be independent of n as the response to the initial deformation is dominated by trapped entanglements and there is likely minimal contribution from the core of the star.  $^{29,31,59,60}$  This reliance on midblock entanglements at low strains should result in similar values for the Young's modulus for materials with equivalent  $f_{PLLA}$ . However, while the 4- and 6-arm stars show comparable stress-strain behavior at small extensions, the Young's moduli for (LLM)<sub>2</sub> is markedly lower than those of (LLM)<sub>4</sub> and (LLM)<sub>6</sub> as well as previously reported triblocks of similar molar mass and composition. The lower Young's modulus observed for the linear triblocks could be due to homopolymer impurities present in these DBU-catalyzed samples, as discussed previously (Figure S10).

Table 2. Mechanical Properties of Star Block Copolymer APTPEs

sample ID $(M_{n,total}, f_{PLLA})$	E <sup>a</sup> (MPa)	$\sigma_{_{ m B}}^{}a}$ (MPa)	ε <sub>B</sub> (%)	tensile toughness <sup>a</sup> (MJ m <sup>-3</sup> )	residual strain <sup>b</sup> (%)	strain recovery	$\Delta H_{\rm m}{}^d$ (J g <sup>-1</sup> )	$\phi_{\mathrm{c}}{}^{e}$
(LLM) <sub>2</sub> (67, 0.17)	$0.95 \pm 0.06$	$14.6 \pm 1.5$	$1454 \pm 53$	91 ± 8	30–36	88–90	3.4	0.18
(LLM) <sub>2</sub> (69, 0.22)	$1.8 \pm 0.4$	$15.2 \pm 0.9$	$1281 \pm 67$	$79 \pm 9$	33–36	88–89	4.1	0.17
$(LLM)_2$ (149, 0.20)	$0.4 \pm 0.1$	$12.1 \pm 1.4$	$1658 \pm 60$	$86 \pm 8$	39–45	85–87	3.7	0.17
(LLM) <sub>2</sub> (197, 0.20)	$0.5 \pm 0.3$	$16.4 \pm 1.2$	$1697 \pm 96$	$98 \pm 10$	36–39	87–88	0.8	0.04
(LLM) <sub>4</sub> (70, 0.17)	$3.2 \pm 0.2$	$5.4 \pm 0.9$	$952 \pm 85$	$37 \pm 10$	27–30	90–91	5.1	0.28
(LLM) <sub>4</sub> (74, 0.22)	$3.9 \pm 0.7$	$12.0 \pm 1.6$	$1026 \pm 66$	$58 \pm 5$	30–33	88–89	4.4	0.20
(LLM) <sub>4</sub> (138, 0.17)	$2.3 \pm 0.1$	$27.3 \pm 1.3$	$1294 \pm 28$	$135 \pm 4$	21–27	91–93	2.9	0.16
(LLM) <sub>4</sub> (147, 0.22)	$4.5\pm0.1$	$31.2 \pm 1.8$	$1419 \pm 45$	$180 \pm 11$	18–24	92–94	1.8	0.08
(LLM) <sub>6</sub> (68, 0.17)	$2.2\pm0.3$	$1.8 \pm 0.1$	$178 \pm 13$	$2.4 \pm 0.3$			5.9	0.32
(LLM) <sub>6</sub> (73, 0.22)	$2.9 \pm 0.3$	$2.1 \pm 0.2$	$161 \pm 17$	$2.3 \pm 0.4$			8.1	0.44
(LLM) <sub>6</sub> (196, 0.17)	$2.2\pm0.2$	$28.7 \pm 0.7$	$1499 \pm 62$	$165 \pm 12$	21–24	92–93	2.2	0.12
(LLM) <sub>6</sub> (214, 0.22)	$5.3 \pm 0.6$	$33.1 \pm 1.3$	$1387 \pm 45$	193 ± 15	24–30	90–92	2.1	0.09

<sup>a</sup> Average values and standard deviations are reported for tensile tests of at least 5 samples extended at 50 mm min<sup>-1</sup> until failure; tensile toughness was calculated from the area under the stress–strain curve. <sup>b</sup> The residual strain was taken to be the percent strain at which the sample exhibited zero stress on the 10th extension cycle. <sup>c</sup> Strain recovery calculated by using the equation  $100 \times$  (applied strain–residual strain)/applied strain. <sup>d</sup> Enthalpy of melting taken as the area under the melting endotherm during the first heat in DSC at a heating rate of  $10 \,^{\circ}$ C min<sup>-1</sup>. <sup>e</sup> calculated using the equation  $\phi_c = \Delta H_m/(w_{\rm PLLA} \times \Delta H_m^{\infty})$ ,  $\Delta H_m^{\infty} = 93 \,^{\circ}$ J g<sup>-1</sup> and  $w_{\rm PLLA}$  is the weight fraction of PLLA.



**Figure 5.** Representative stress-strain curves comparing star block polymers (LLM)<sub>n</sub> with constant  $M_{arm}$  where n = 2 (black), 4 (red), and 6 (blue) with  $f_{PLLA} = 0.17$  (top) and  $f_{PLLA} = 0.17$  (bottom). The curves are representative from five melt-pressed dog bones pulled at 50 mm min<sup>-1</sup> to the sample break point, indicated by  $\times$ .

The (LLM)<sub>4</sub> and (LLM)<sub>6</sub> star polymers displayed improved stress-strain behavior compared to (LLM)<sub>2</sub> samples. The 4- and 6-arm star APTPEs exhibited more pronounced strain

hardening than the linear triblock, resulting in significantly higher ultimate tensile strengths (Figure 6a). In contrast to previous reports,  $^{28,29,31,38}$  this increase in tensile strength was not accompanied by a concurrent decrease in the elongation at break (Figure 6b), leading to much higher tensile toughness values for (LLM)4 and (LLM)6 compared to (LLM)2 samples. Molecular dynamics simulations by Parker and Rottler<sup>59</sup> exploring uniaxial tensile deformation in sphereforming (AB)n star block polymers have predicted that the onset of strain hardening occurs at smaller strains as the number of arms increases. The stress-strain curves of the 4- and 6-arm star APTPEs with  $f_{PLLA} = 0.22$  show this behavior; however, the stars with  $f_{PLLA} = 0.17$  display the opposite trend, with the onset of strain-hardening in the 4-arm stars occurring at ~50% smaller strains than in the 6-arm star for reasons that are not immediately apparent.

Both the 4- and 6-arm stars displayed impressive ultimate tensile strengths, outperforming a commercially available styrenic TPE with comparable molar mass and hard block content, Kraton<sup>TM</sup> D1111 (Figure 6a). The observed improvement in the ultimate tensile strength as a result of the star architecture agrees with literature precedent.<sup>28-31</sup> Additionally, the smaller PLLA domain sizes observed in the 4- and 6-arm star polymers indicates that there are more hard domains per unit volume in the star polymers than in the linear triblocks. These more highly dispersed PLLA domains are predicted to result in an increased degree of hard domain interconnectedness in the star polymers (i.e., more hard domains connected through intervening rubbery midblocks) and a subsequent enhancement in the ultimate tensile strength. Interestingly, the ultimate tensile strengths of (LLM)<sub>4</sub> and (LLM)<sub>6</sub> are similar, suggesting that these APTPE star polymers may reach a plateau in the ultimate tensile strength at an arm functionality of 4 rather than the range of n = 5-10 that has been observed in previously studied star polymer systems. <sup>28,29,32</sup> Simulations by Spencer and Matsen<sup>60</sup> have shown that (AB)<sub>n</sub> star polymers display an increased fraction of bridging chains (e.g., chains that connect two discrete hard domains) compared to linear ABA

triblocks. As the number of arms increases, the proportion of these bridging chains also rapidly increases, and they suggest for  $(AB)_n$  stars with a spherical or cylindrical morphology almost all stars form bridges once n = 9. The similarity between the observed tensile behaviors (i.e., ultimate tensile strength and toughness) in the 4- and 6-arm  $(LLM)_n$  samples suggests that the APTPE stars may reach a mechanically relevant fraction of bridging chains at a lower arm number as compared to the cyclosiloxane and divinyl benzene cores that are typically employed for PS-containing star TPEs.  $^{28,29,56,61}$ 

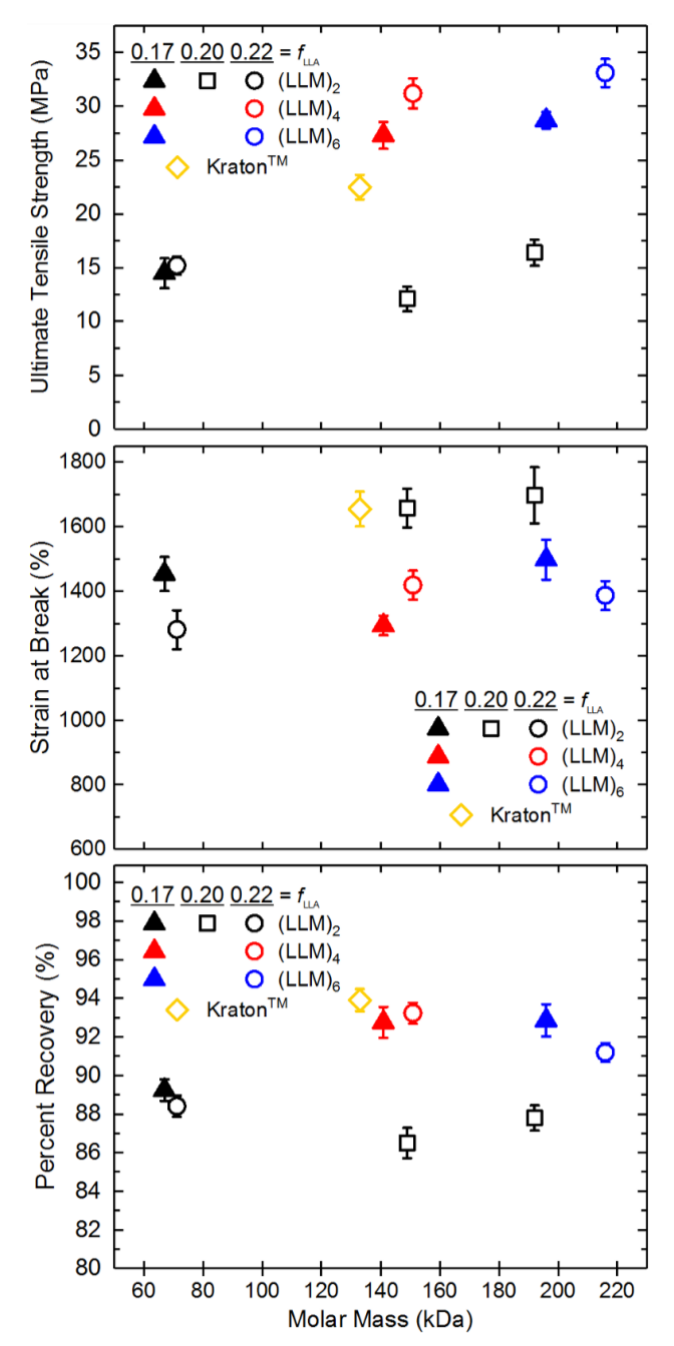


**Figure 6.** Mechanical properties: (a) ultimate tensile strength ( $\sigma_B$ ), (b) strain at break, and (c) percent recovery of star block copolymers (LLM)<sub>n</sub> of constant arm molar mass with  $f_{PLLA} = 0.17$  (solid triangle), 0.20 (open square) and 0.22 (open circle) and n arms where n = 2 (black), n = 4 (red), and n = 6 (blue) compared to a commercial Kraton<sup>TM</sup> SIS with  $f_{PS} = 0.15$ –0.19. Samples

were extended at 50 mm min<sup>-1</sup> with percent recovery calculated from residual strain after 10 cycles of 300% strain.

The star APTPEs were subjected to cyclic loadings of 300% strain at 50 mm/min for 10 cycles to explore their hysteresis and recovery behavior. Figure 6c shows the strain recovery of the APTPEs (recovered strain as a percentage of the applied 300% strain after 10 cycles) calculated using the residual strain (strain when the material exhibits zero stress) after 10 cycles. Experiments were run in triplicate, and the range of values collected are reported in Table 2. All of the APTPEs display elastomeric behavior with ≥ 85% strain recovery. The 4- and 6-arm star polymers exhibited superior recovery than the linear APTPEs, displaying similar stain recoveries in the range of 90–94%. These data suggest that the covalent-crosslink at the core of the star facilitates improved recovery behavior.<sup>31</sup>

To further explore the impact of the star architecture on elastomeric properties and material deformation, the stress relaxation behavior of (LLM)<sub>2</sub>, (LLM)<sub>4</sub>, and (LLM)<sub>6</sub> were compared. Samples were equilibrated at 40 °C for 10 min before the application of a 25% step-strain, and the resulting stress response was monitored over 3 h ( $10^4$  s) (Figure 7). Based on our previous work, a temperature of 40 °C was selected to best highlight the impact of architectural changes on the stress relaxation behavior. The APTPEs with  $f_{PLLA} = 0.22$  relax less stress than those with  $f_{PLLA} = 0.17$ , likely due to the increased molar mass of the PLLA domains (Figure 7). For both  $f_{PLLA}$  studied, the 4- and 6-arm stars exhibited significantly improved stress relaxation behavior compared to the linear triblock. Matsen<sup>41,62</sup> has shown that the segregation strength in (AB)<sub>n</sub> type block copolymers should be calculated using  $N_{arm}$  rather than  $N_{total}$ , indicating that, despite their different molar masses, the segregation strength of the 2-, 4-, and 6-arm star polymers are comparable (Table S1). This suggests that the improvement in the stress relaxation behavior

observed in the star polymers is a result of the star architecture. We posit that this improvement is due to the ability of the permanent crosslink at the core of the star to mitigate the impact of chain pullout of a PLLA block from a hard domain.  $^{9,15,18,20,31,63}$  In a linear triblock, chain pullout of a PLLA end block results in the release of trapped entanglements, decreasing the functionality of the physical crosslinks and leading to increased permanent set and hysteresis. However, for the star block polymers, chain pullout results in the relaxation of only the failed arm, as the other arms remain anchored to the network, maintaining elastically effective connections between the hard domains. This effect is further enhanced by the increased number of bridging chains in the star architecture compared to linear triblocks. The introduction of a star architecture results in less stress relaxation; however, the 4- and 6-arm stars both relax approximately 50–60% of the original stress after 3 h, indicating that the stress relaxation behavior is independent of arm functionality. These data agree with the comparable  $\chi N$  values among the star polymers as well as previous reports suggesting that for star homopolymers with low arm numbers (n<8) the stress relaxation is independent of arm functionality.

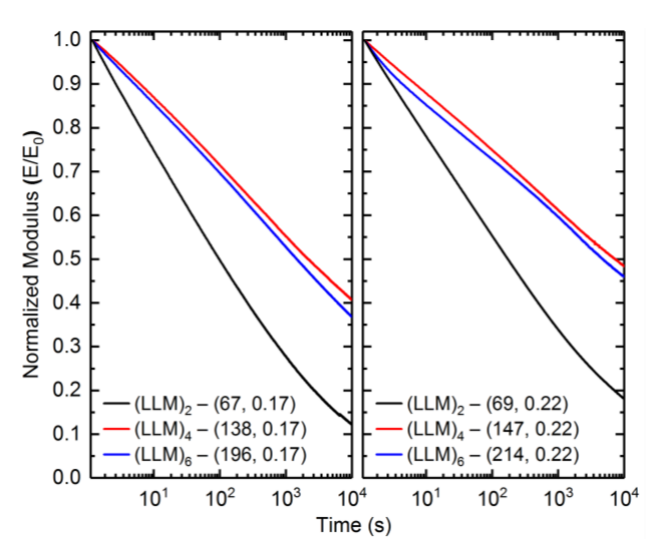


**Figure 7.** Stress relaxation of (LLM)<sub>n</sub> star block polymers with n = 2 (black), n = 4 (red), and n = 6 (blue) and  $f_{PLLA} = 0.17$  (left) and 0.22 (right) at 40 °C. Samples were held at a 25% strain for 3 h. The modulus values have been normalized to allow for comparison between samples.

The above experiments demonstrate that the implementation of a star architecture in these APTPEs results in significant improvement in mechanical properties as compared to their linear 2-arm "star" analogues. These data suggest that the introduction of a chemical crosslink at the core of the star is the major contributor to improved material performance, with increasing star functionality from 4 to 6 not significantly impacting observed behavior. We next explored high-molar-mass linear analogues of the 4- and 6-arm stars to help distinguish the impact of the increase in molar mass with increasing arm number from architectural effects.

Mechanical Performance of High-Molar-Mass Poly(L-lactide)-b-poly(γ-methyl-ε-caprolactone)-b-poly(L-lactide) Analogues.

The mechanical performance of ABA TPEs, particularly their tensile properties, are highly dependent on molar mass due to its impact on both segregation strength between blocks ( $\chi N$ ) and

number of midblock entanglements. As such, high molar masses are typically required to achieve well-segregated, high-performance materials. To decouple effects resulting from the increased molar masses in the 4- and 6-arm stars from the impact of the star architecture, a series of high-molar-mass linear (2-arm) analogues with comparable overall molar masses to the star samples were synthesized (Table 1). The high-molar-mass linear analogues were processed in the same manner as described previously and their mechanical properties investigated. DSC traces display glass transitions for both the PγMCL and PLLA blocks as well as the PLLA melting endotherm, suggesting that the materials are microphase separated. This is further supported by DMTA traces of the polymers up to 190 °C, which do not display a precipitous drop in the modulus characteristic of the *T*<sub>ODT</sub> as well as variable temperature SAXS analysis (Figures S23–S25).

The mechanical properties of the high-molar-mass linear polymers were characterized using extensional DMTA and compared to 4- and 6-arm stars of similar molar mass (Figure 8). All samples display the expected drop in modulus near -57 °C due to the P $\gamma$ MCL glass transition and the plateau modulus (E' = 3–4 MPa) is consistent between samples. All samples maintain the plateau modulus upon heating until approximately 60 °C where there is a small dip in the modulus due to the glass transition of PLLA. As was observed previously, the plateau modulus for all samples then begins to gradually decrease upon continued heating. The 4- and 6-arm stars maintain their plateau modulus to higher temperatures than the linear analogues, softening at 176 °C and > 190 °C (i.e., the samples did not soften during tested range), respectively. (LLM)<sub>2</sub> (149, 0.20) softens at 135 °C, near the  $T_m$  of PLLA as observed using DSC; however, the (LLM)<sub>2</sub> (197, 0.20) sample maintains the plateau modulus up to 145 °C, the  $T_m$  of PLLA, where it begins to decrease steeply until failure at 180 °C. This softening temperature is above the expected  $T_m$  of the sample

as analyzed by DSC, but may be influenced by the increased number of entanglements in the  $P\gamma$ MCL and PLLA blocks due to their high molar masses.

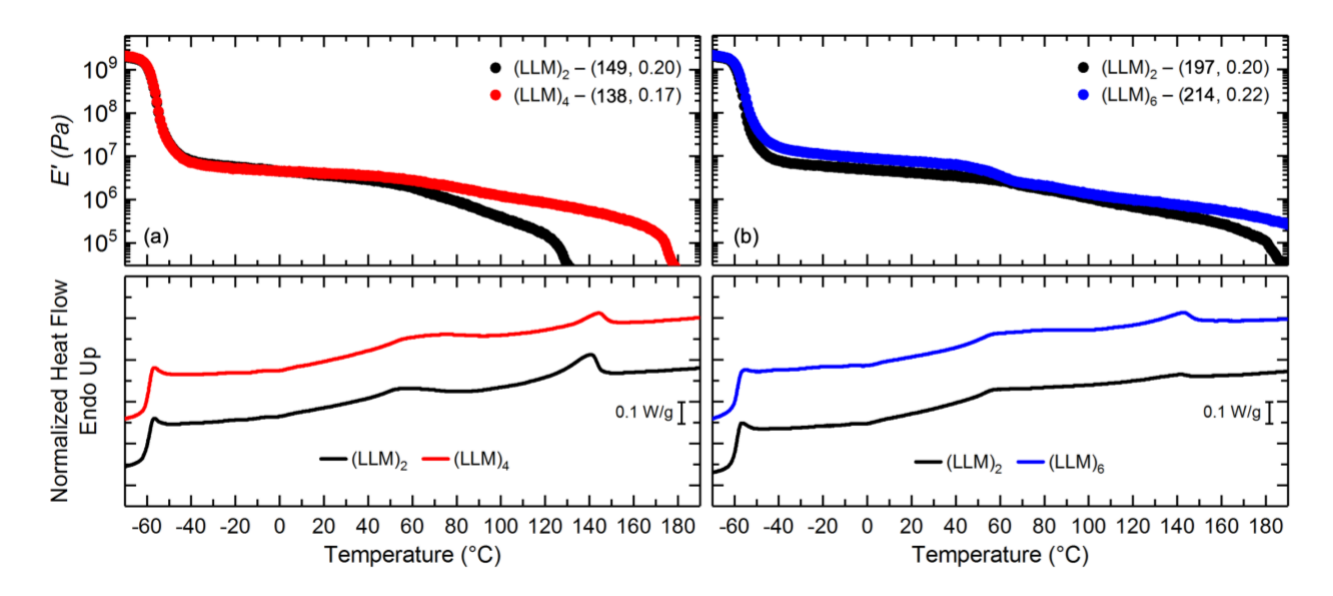


**Figure 8.** Thermal properties of (LLM)<sub>n</sub> with (a)  $M_{\text{polymer}} \approx 140 \text{ kDa}$  and (b)  $M_{\text{polymer}} \approx 210 \text{ kDa}$  where n = 2 (black), 4 (red), and 6 (blue) analyzed by DMTA in tension upon heating at 5 °C min<sup>-1</sup> (top, 1 Hz, 0.05% strain) and DSC upon heating at 10 °C min<sup>-1</sup> (bottom).

The stress-strain behavior of (LLM)<sub>2</sub> (149, 0.20) and (LLM)<sub>2</sub> (197, 0.20) is quite distinct as compared to that of the 4- and 6-arm stars at comparable molar mass (Figure 9). The high-molar-mass linear polymers displayed impressive elongations at break ( $\varepsilon_B = 1650-1800\%$ ). As expected, and the ultimate tensile strength of (LLM)<sub>2</sub> (197, 0.20) ( $\sigma_B = 16.4 \pm 1.2$  MPa) was greater than that of (LLM)<sub>2</sub> (149, 0.20) ( $\sigma_B = 12.1 \pm 1.4$ ). However, despite the increase in molar mass, the observed ultimate tensile strengths for the high-molar-mass triblocks were dramatically lower than those of the 4- and 6-arm star polymers ( $\sigma_B = 27-33$  MPa) (Figure 6a). These data indicate that the improvement in the ultimate tensile properties observed in the 4- and 6-arm star polymers

compared to the linear TPEs with equivalent  $M_{arm}$  is due to the star architecture rather than the increase in molar mass. Additionally, the high-molar-mass "2-arm" triblocks did not show enhanced strain recovery behavior when compared to the 4- and 6-arm star polymers, displaying residual strains (0.36–0.45) comparable to the low-molar-mass triblocks (Figure 6c, Table 2).

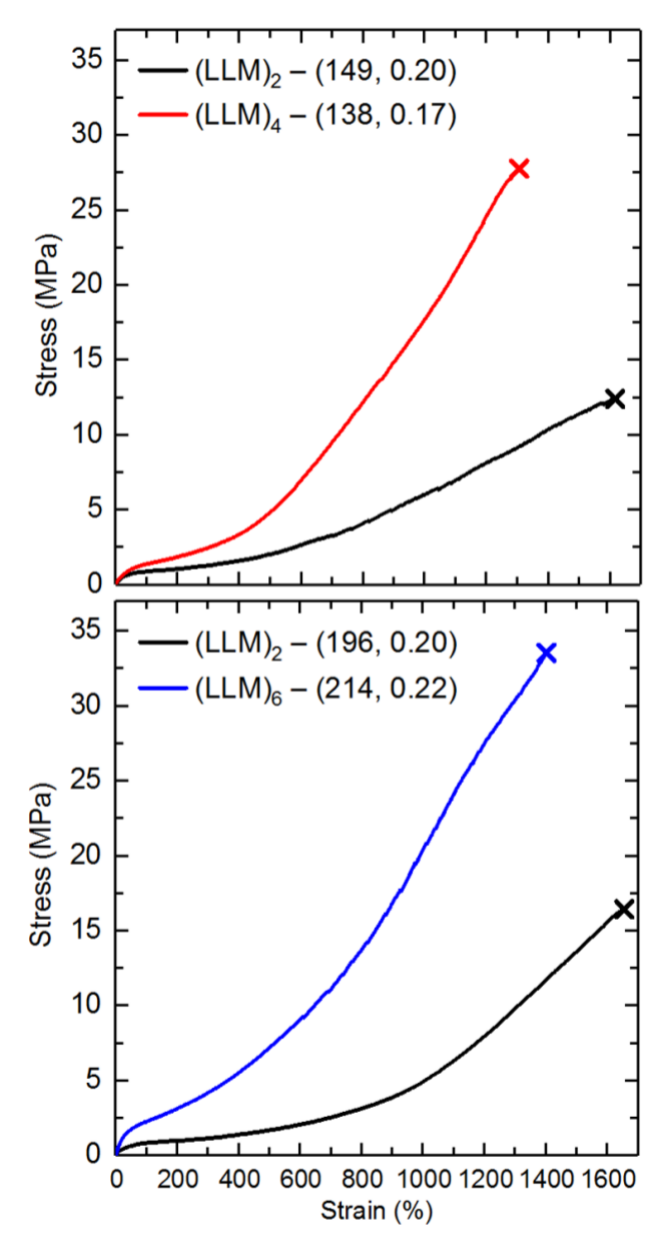


**Figure 9.** Representative stress-strain curves comparing star block polymers (LLM)<sub>n</sub> with constant  $M_{polymer}$  ( $M \approx 140$  kDa, top;  $M \approx 210$  kDa, bottom) where n = 2 (black), 4 (red), and 6 (blue). The curves are representative from five melt-pressed dog bones pulled at 50 mm min<sup>-1</sup> to the sample break point, indicated by  $\times$ .

As expected, the high-molar-mass triblocks show improved stress relaxation behavior compared to the low-molar-mass triblocks, relaxing around 70% of the applied stress after 3 h at

40 °C. This improvement is likely due to the increased number of entanglements in both the glassy and rubbery domains as well as a larger segregation strength between blocks (i.e., higher  $\chi N$ ). Even so, both the 4- and 6-arm stars relax less stress than their linear analogues, losing 50% and 60%, respectively, of the original stress after 3 h at 40 °C (Figure 10). For comparison, the stress relaxation behavior of these multi-arm star APTPEs is on par with a commercial styrenic SIS TPE, Kraton<sup>TM</sup> D1111, which relaxes 45% of the applied stress under the same conditions. Despite their analogous molar masses, the segregation strengths of the star polymers ( $\chi N \approx 45$ ) are considerably lower than that of the high-molar-mass linear triblocks ( $\chi N = 96$ , 127) (Table S1) suggesting that the improvement in the stress relaxation behavior observed in the star polymers is a result of the star architecture rather than the increased molar mass.<sup>41,63</sup>

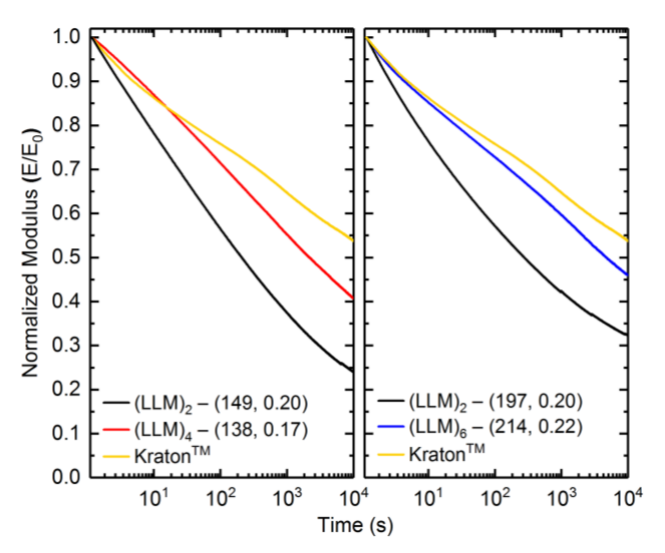


**Figure 10.** Stress relaxation of (LLM)<sub>n</sub> star block polymers with  $M_{polymer} \approx 140$  kDa (left) and  $M_{polymer} \approx 210$  kDa (right) where n = 2 (black), n = 4 (red), and n = 6 (blue) at 40 °C compared to the stress relaxation profile of Kraton<sup>TM</sup> 1111D. Samples were held at a 25% strain for 3 h. The modulus values have been normalized to allow for comparison between samples.

Previous experiments have shown that there are significant differences in the entanglement dynamics and stress relaxation behavior of linear and star polymers.  $^{29,67-71}$  Using an earlier version of the tube model as a foundation,  $^{67}$  the theory for the stress relaxation of star polymer melts developed by Milner and McLeish posits that the core of the star prevents the reptation of the arms that is evident for linear chains.  $^{65}$  As conformational rearrangement via arm retraction occurs in each arm independently, the dynamic behavior of multi-arm stars is independent of the number of arms when  $n \ge 4$ , which agrees with experimental results.  $^{67}$  We posit that chain pullout of the PLLA end blocks from the hard domains is principally responsible for stress relaxation in these APTPEs;  $^{6.9,15,63}$  however, once this failure occurs the free arm of the star must undergo additional configurational rearrangements to release trapped entanglements before re-entering a hard domain as compared to the linear system.

Based on the above experiments we conclude that the improvement in material properties observed in the star polymers is a result of the star architecture rather than increased molar mass. Additionally, they further highlight that the star polymers are more resistant to the effects of impurities than linear triblocks. Overall, these data show that through simple architectural changes, we are able to synthesize high performance materials with competitive properties to commercial styrenic TPEs. We next explored whether this improvement in mechanical performance from the star architecture would also be observed in lower-molar-mass systems.

# Mechanical Performance of Lower-Molar-Mass (poly(L-lactide)-b-poly( $\gamma$ -methyl- $\epsilon$ -caprolactone))<sub>n</sub> Star Polymers

Low-molar-mass 4- and 6-arm star analogues with  $f_{PLLA} = 0.17$  and 0.22 were synthesized as discussed above to investigate whether the benefits from employing a star architecture could be translated to lower-molar-mass systems (Table 1). DSC traces of the samples show glass

transitions for both P $\gamma$ MCL and PLLA as well as a melting transition for the PLLA blocks (Figure 11). The observed  $T_{gS}$  for the PLLA blocks ( $T_{g}$  = 21–32 °C) are lower than that of the high-molar-mass homopolymer due to the low molar masses of the PLLA blocks. The low  $\chi N$  in these 4- and 6-arm star polymers may also lead to some degree of mixing between the PLLA and P $\gamma$ MCL blocks which would result in a depressed  $T_{g}$ . The melting transition in (LLM)<sub>6</sub> (68, 0.17) is bimodal, with  $T_{m}$  values, determined from the peaks of the melting endotherm, at 92 and 128 °C possibly due to the presence of melting–recrystallization events, which can be observed in TPEs with crystallizable blocks.  $^{1,72}$ 

These melting points, as well as the melting point of (LLM)<sub>4</sub> ( $T_{\rm m}$  = 139 °C), are suppressed compared to that of (LLM)<sub>2</sub> ( $T_{\rm m}$  = 145 °C). This depression in  $T_{\rm m}$  is likely due to a combination of the restriction on chain segment mobility due to the star architecture during crystallization and the low molar masses of the PLLA blocks in these samples.

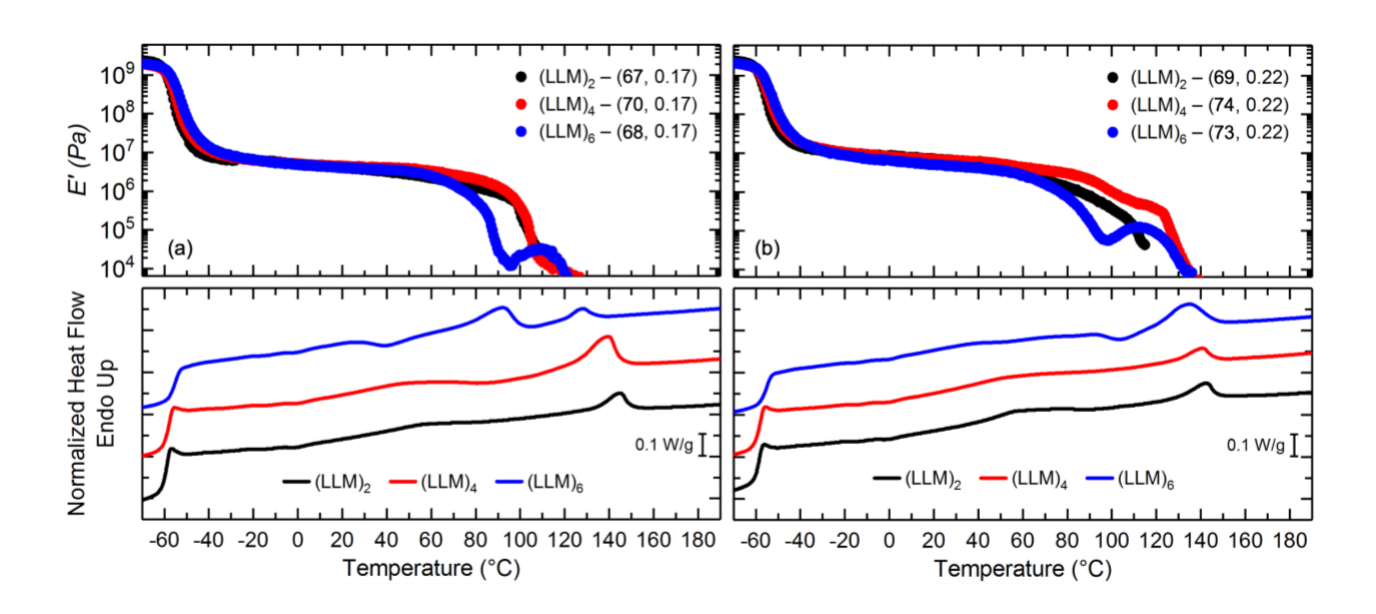


**Figure 11.** Thermal properties of (LLM)<sub>n</sub> where n = 2 (black), 4 (red), and 6 (blue), with (a)  $f_{PLLA} = 0.17$  and (b)  $f_{PLLA} = 0.22$  analyzed by DMTA in tension upon heating at 5 °C min<sup>-1</sup> (top, 1 Hz, 0.05% strain); and DSC upon heating at 10 °C min<sup>-1</sup> (bottom).

Room temperature SAXS patterns of the samples are shown in Figures S27–S29 The 4-and 6-arm star polymers display broad, low intensity principal scattering peaks with no higher order reflections, suggestive of a disordered morphology. The impact of a low  $T_{\rm ODT}$  on the crystallization behavior of these polymers is discussed in more detail in the Supporting Information. At a constant molar mass, increasing the number of arms results in a decrease in the length of the P $\gamma$ MCL and PLLA blocks, which leads to smaller domain spacings as the star functionality increases. As a result, there is a dramatic increase in the number of hard domains per unit volume for these low-molar-mass APTPEs as the number of arms is increased from 2 to 4 to 6 (Table 1).

The mechanical properties of the low-molar-mass star polymers were characterized by extensional DMTA (Figure 11). As seen in the previous samples, there is a drop in the modulus at -56 °C due to the glass transition of P $\gamma$ MCL, and the modulus of the rubbery plateau is consistent between samples (E' = 3–5 MPa). The 2- and 4-arm star polymers all perform similarly, maintaining the plateau modulus upon heating until a steep drop in E' near 120 °C, close to the PLLA  $T_{\rm m}$  for the samples as seen in the DSC traces. Unlike (LLM)<sub>2</sub> or (LLM)<sub>4</sub>, the 6-arm stars begin to soften around 80 °C, leading to a drop in the modulus that is then partially recovered upon further heating before final material failure around 120 °C. Comparison of this behavior with corresponding DSC traces indicates that the samples are first undergoing melting at 80 °C followed by crystallization and then final melting of the PLLA crystallites at 120 °C. This conclusion was

further corroborated by shear rheology experiments. Shear DMTA traces for the 6-arm stars similarly display a recoverable dip in the modulus beginning at 80 °C that is reproducible across multiple heating and cooling cycles (Figure S32). Further frequency sweeps demonstrate that PLLA crystallization in these samples can be promoted through annealing at 100 °C (Figure S33). The behavior observed in the 6-arm star polymers suggests that the low PLLA molar masses in these materials influences the crystallization kinetics and promotes increased crystallization. This is further supported by the higher degrees of crystallinity observed in the low-molar-mass (LLM)6 and (LLM)4 materials compared to the linear triblocks or high-molar-mass stars (Table 2).

Unlike their high-molar-mass analogues, the low-molar-mass 4- and 6-arm stars do not exhibit strain hardening behavior, likely due to the short PLLA chains and disordered morphology, which results in significantly lower ultimate tensile strengths compared to the analogous linear triblock (Figure S35). (LLM)<sub>6</sub> (68, 0.17) displayed the lowest ultimate tensile strengths of all polymers studied ( $\sigma_B = 1.8 \pm 0.1$  MPa) and failed at small extensions ( $\epsilon_B = 178 \pm 13\%$ ). (LLM)<sub>4</sub> (70, 0.17) exhibited moderately improved ultimate tensile strengths ( $\sigma_B = 5.4 \pm 0.9$  MPa) and significantly larger elongations at break ( $\epsilon_B = 952 \pm 85\%$ ). Increasing the  $f_{PLLA}$  to 0.22 did not significantly impact the performance of the 6-arm stars; however, the 4-arm stars displayed markedly increased ultimate tensile strengths of ~12 MPa (Figure 12a). The linear triblocks of low molar mass outperform the star polymers of equivalent molar mass with respect to both ultimate tensile strength and elongation at break(Figure 12a,b). The low elongations at break observed for the low-molar-mass 6-arm star polymers prevented the samples from withstanding testing without failure and as such the recovery properties are not reported. In contrast, (LLM)<sub>4</sub> (70, 0.17) and (LLM)<sub>4</sub> (74, 0.22) both display elastomeric behavior, exhibiting recoveries of 91 and 89%.

respectively (Figure 12c). This recovery behavior is on par with that of the linear TPEs, and further suggests that the core of the star acts to provide additional memory to the network.

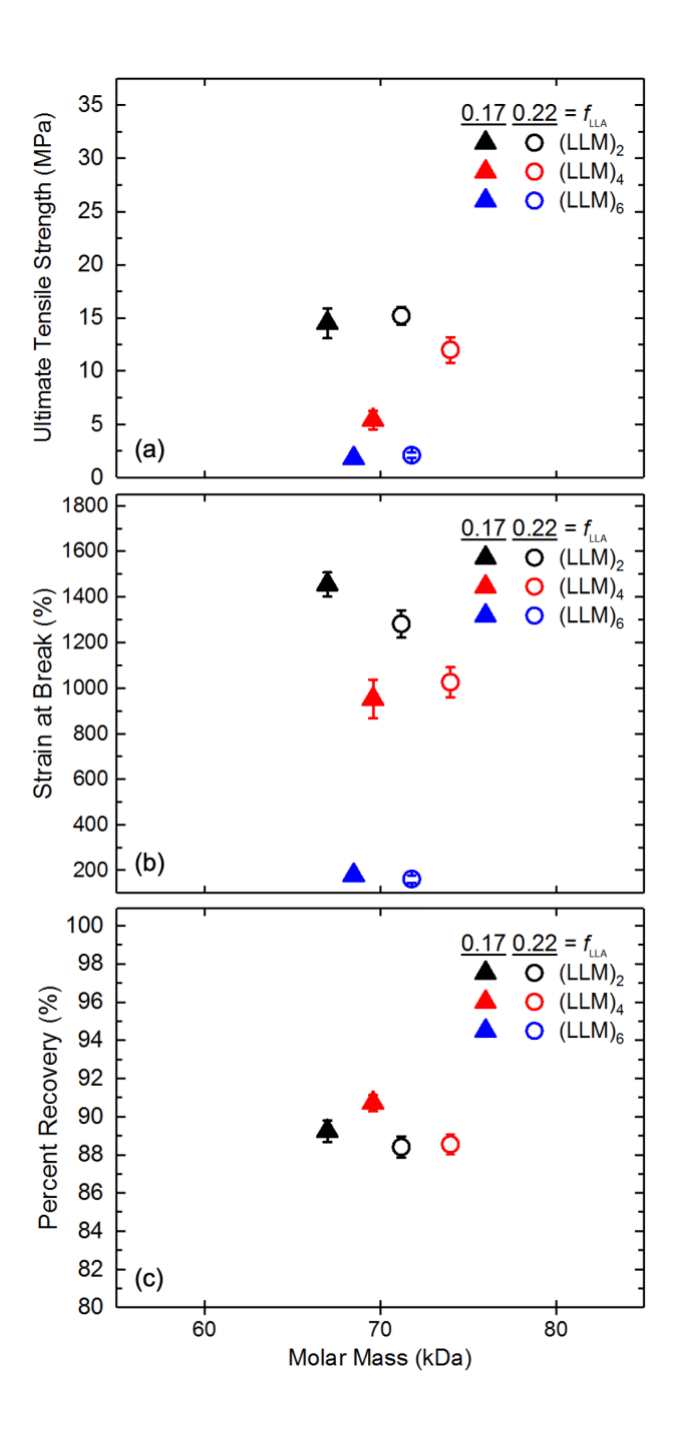


**Figure 12.** Mechanical properties: (a) ultimate tensile strength, (b) strain at break, and (c) percent recovery of star block copolymers, (LLM)<sub>n</sub>, with  $f_{PLLA} = 0.17$  (solid triangle) and 0.22 (open circle) and n arms where n = 2 (black), n = 4 (red), and n = 6 (blue). Samples were extended at 50 mm min<sup>-1</sup> with percent recovery calculated from residual strain after 10 cycles of 300% strain.

While (LLM)<sub>4</sub> (74, 0.22) displays a moderate performance, all other low-molar-mass star polymers exhibit poor tensile properties with low ultimate tensile strengths. The decline in the tensile properties with increasing arm number is likely a consequence of the decrease in segregation strength (i.e.,  $\chi N \approx 45$ ,  $\chi N \approx 23$ ,  $\chi N \approx 15$ , for n=2, 4, and 6, respectively), which can lead to mixing between the hard and soft blocks and result in diffuse interfaces between the hard and soft domains.<sup>73</sup> The less well-defined hard domains in these more weakly segregated systems may lead to untrapped entanglements and more facile chain failure. Additionally, any crystallization-inducted microphase separation in such weakly segregated systems would be expected to impact material properties.<sup>10</sup>

The stress relaxation behavior of the low-molar-mass star polymers was investigated and compared to the linear triblocks (Figure 13). The 6-arm star polymers both underwent brittle fracture during testing, likely due to the weak segregation in these samples. Interestingly, the low-molar-mass 4-arm star polymers exhibit impressive stress relaxation behavior, outperforming both the analogous linear triblocks and the high-molar-mass stars. (LLM)4 (70, 0.17) displays the least amount of stress relaxation of all samples studied, losing only 25% of the original stress after 3 h. As a comparison, the high-molar-mass styrenic TPE, Kraton<sup>TM</sup> D1111, relaxes 45% of the applied stress. DSC studies of (LLM)<sub>2</sub> (67, 0.17) before and after testing do not show an increase in the enthalpy of fusion of the first heating cycle, indicating that this stress relaxation behavior is not a

result of PLLA crystallization during testing (Figure S36). While these low-molar-mass 4-arm stars display inferior tensile properties when compared to their linear analogues, they exhibit significantly less stress relaxation, even outperforming commercial materials (Figure S37).

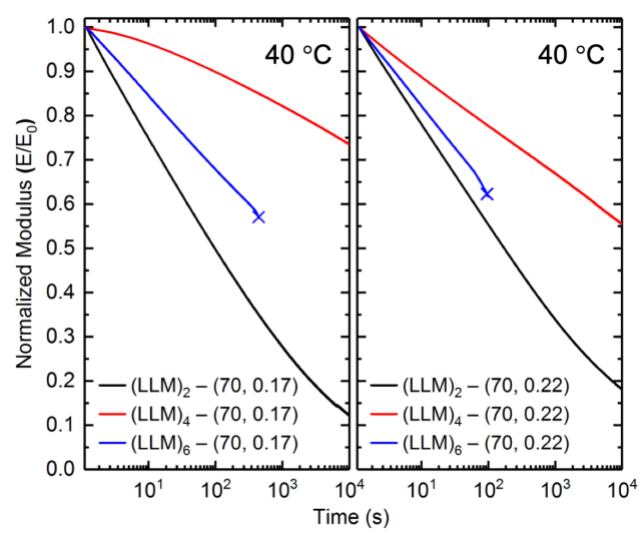


**Figure 13.** Stress relaxation of (LLM)<sub>n</sub> star block polymers where n = 2 (black), n = 4 (red), and n = 6 (blue) and  $f_{PLLA} = 0.17$  (left) and 0.22 (right) at 40 °C. Samples were held at a 25% strain for 3 h. The modulus values have been normalized to allow for comparison between samples, and material break point is indicated by  $\times$ .

## **Conclusions**

We have demonstrated the efficient, one-pot, two step synthesis of a series of aliphatic polyester star block TPEs. The selection of catalyst influences the nature and level of impurities present in the system and the mechanical properties of the resulting polymers. The multi-arm star APTPEs displayed more resilience to these impurities compared to linear analogues, emphasizing a benefit of the star architecture. SAXS studies of the materials indicate that the star polymers are microphase-separated at room temperature, with no evidence of crystalline breakout, and display smaller domain spacings than linear materials with analogous  $M_{arm}$ . At a constant  $M_{arm}$ , the star architecture gave significant improvements in ultimate tensile strength, tensile toughness, and

strain recovery compared to analogous linear triblocks (2-arm "stars"). The star APTPEs also outperformed a commercial styrenic material in these categories, highlighting competitive properties to current commodity materials. Comparison to linear analogues of comparable overall molar mass indicates that this improvement in tensile behavior is a feature of the star architecture rather than an effect of increased molar mass by virtue of the increased number of arms. The increase in ultimate tensile strength and improved recovery is likely due to the chemical crosslink at the core of the star which more evenly distributes applied stresses across the network, as well as the greater number of hard domains per unit volume in the star polymers compared to linear analogues. While the star architecture resulted in improved tensile properties at high-molarmasses, 4- and 6-arm stars with constant lower molar masses underperform their linear analogues with respect to both ultimate tensile strength and strain at break. This decreased tensile performance potentially underlines the impact of segregation strength ( $\chi N_{arm}$ ) on material properties in these star APTPEs and suggests that there is a critical molar mass at which the star architecture becomes advantageous over linear analogues. The star architecture also results in improved stress relaxation behavior. The 4- and 6-arm stars with constant  $M_{arm}$  relax less stress than their linear analogues of both analogous  $M_{arm}$  and overall molar mass.

This work has shown that we are able to further enhance the material performance in these high performance APTPEs through the straightforward implementation of a star architecture. At sufficient molar masses, the star architecture results in materials with increased ultimate tensile strengths and improved recoveries that outperform commercially available styrenic TPEs. The star architecture has also been shown to mitigate the impact of chain pullout and result in materials with slow stress relaxation and minimal permanent deformation. The enhanced understanding of the relationship between polymer architecture and material properties from this work will allow for further improvements in the design of high performance sustainable APTPEs.

# Acknowledgements

We would like to acknowledge Daphne Wui Yarn Chan, Steven Weigand, and Gabriela Diaz Gorbea for collecting SAXS data as well as Farihah Haque, Colin Peterson, Jay Weber, Annabelle Watts, Mahesh Mahanthappa, and Elizabeth Feinberg for many helpful discussions. We thank Ortec, Inc. for generously providing lactide used in these studies. SAXS experiments were performed at the DuPont-Northwestern-Dow Collaborative Access Team (DND-CAT) located at Sector 5 of the Advanced Photon Source (APS). DND-CAT is supported by the Northwestern University, E.I. DuPont de Nemours & Co., and Dow Chemical Company. This research used resources of the Advanced Photon Source, a U.S. Department of Energy (DOE) Office of Science user facility operated for the U.S. DOE Office of Science by the Argonne National Laboratory under contract no. DE-AC02-06CH11357. Graphics creation was assisted by John Beumer with the NSF Center for Sustainable Polymers. We also acknowledge the funding for this work, which was provided by the NSF Center for Sustainable Polymers (CHE-1901635) at the University of Minnesota.

#### **Associated Content**

### **Supporting Information**

Materials and methods; detailed synthetic procedures and characterization details; <sup>1</sup>H NMR spectra, DMTA data, DSC data, SEC data, tensile data, stress relaxation data, and SAXS spectra (Table S1 and Figures S1–S37).

## References

(1) Holden, G.; Kricheldorf, H. R.; Quirk, R. P. *Thermoplastic Elastomers*, 3rd ed.; Holden,

- G., Kricheldorf, H. R., Quirk, R. P., Eds.; Hanser Gardner Publications, Inc.: Cincinnati, 2004.
- (2) Tong, J. D.; Jerôme, R. Dependence of the Ultimate Tensile Strength of Thermoplastic Elastomers of the Triblock Type on the Molecular Weight between Chain Entanglements of the Central Block. *Macromolecules* **2000**, *33* (5), 1479–1481.
- (3) Reisch, M. S. Thermoplastic Elastomers Target Rubber And Plastics Markets. *Chemical & Engineering News*. August 1996, pp 10–14.
- (4) Holden, G.; Bishop, E. T. T.; Legge, N. R. R. Thermoplastic Elastomers. *J. Polym. Sci. Part C Polym. Symp.* **1969**, *26* (1), 37–57.
- (5) Martello, M. T.; Hillmyer, M. A. Polylactide-Poly(6-Methyl-ε-Caprolactone)-Polylactide Thermoplastic Elastomers. *Macromolecules* **2011**, *44* (21), 8537–8545.
- (6) Martello, M. T.; Schneiderman, D. K.; Hillmyer, M. A. Synthesis and Melt Processing of Sustainable Poly(ε-Decalactone)-Block-Poly(Lactide) Multiblock Thermoplastic Elastomers. ACS Sustain. Chem. Eng. 2014, 2 (11), 2519–2526.
- (7) Hillmyer, M. A.; Tolman, W. B. Aliphatic Polyester Block Polymers: Renewable, Degradable, and Sustainable. *Acc. Chem. Res.* 2014, 47 (8), 2390–2396.
- (8) Schneiderman, D. K.; Hillmyer, M. A. 50th Anniversary Perspective: There Is a Great Future in Sustainable Polymers. *Macromolecules* **2017**, *50* (10), 3733–3749.
- (9) Watts, A.; Kurokawa, N.; Hillmyer, M. A. Strong, Resilient, and Sustainable Aliphatic Polyester Thermoplastic Elastomers. *Biomacromolecules* 2017, 18 (6), 1845–1854.
- (10) Watts, A.; Hillmyer, M. A. Aliphatic Polyester Thermoplastic Elastomers Containing Hydrogen-Bonding Ureidopyrimidinone Endgroups. *Biomacromolecules* **2019**, *20* (7),

- 2598–2609.
- (11) Schneiderman, D. K.; Hillmyer, M. A. Aliphatic Polyester Block Polymer Design. *Macromolecules* **2016**, *49* (7), 2419–2428.
- (12) Xiong, M.; Schneiderman, D. K.; Bates, F. S.; Hillmyer, M. A.; Zhang, K. Scalable Production of Mechanically Tunable Block Polymers from Sugar. *Proc. Natl. Acad. Sci.* 2014, 111 (23), 8357–8362.
- (13) Wanamaker, C. L.; O'Leary, L. E.; Lynd, N. A.; Hillmyer, M. A.; Tolman, W. B.; Hillmeyer, M. A.; Tolman, W. B. Renewable-Resource Thermoplastic Elastomers Based on Polylactide and Polymenthide. *Biomacromolecules* 2007, 8 (11), 3634–3640.
- (14) Schneiderman, D. K.; Hill, E. M.; Martello, M. T.; Hillmyer, M. A. Poly(Lactide)-Block-Poly(ε-Caprolactone-Co-ε-Decalactone)-Block-Poly(Lactide) Copolymer Elastomers. *Polym. Chem.* **2015**, *6* (19), 3641–3651.
- (15) Hotta, A.; Clarke, S. M.; Terentjev, E. M. Stress Relaxation in Transient Networks of Symmetric Triblock Styrene-Isoprene-Styrene Copolymer. *Macromolecules* **2002**, *35* (1), 271–277.
- (16) Gent, A. N. Relaxation Processes in Vulcanized Rubber. I. Relation among Stress Relaxation, Creep, Recovery, and Hysteresis. J. Appl. Polym. Sci. 1962, 6 (22), 433–441.
- (17) López-Barrón, C. R.; Eberle, A. P. R.; Yakovlev, S.; Bons, A. J. Structural Origins of Mechanical Properties and Hysteresis in SIS Triblock Copolymers/Polystyrene Blends with Spherical Morphology. *Rheol. Acta* 2016, 55 (2), 103–116.
- (18) Hsiue, G.-H.; Wu, G.-W. The Stress Relaxation of the Thermoplastic Elastomer (SBS Type). *J. Appl. Polym. Sci.* **1980**, *25* (9), 2119–2121.

- (19) Hsiue, G.-H; Chen, D.-J; Liew, Y.-K. Stress Relaxation and the Domain Structure of Thermoplastic Elastomer. *J. Appl. Polym. Sci.* **1988**, *35* (4), 995–1002.
- (20) Spaans, R. D.; Williams, M. C. Nonlinear Viscoelasticity of ABA Block Copolymer Melts: Stress Relaxation and Recovery. *Ind. Eng. Chem. Res.* 1995, 34 (10), 3496–3507.
- (21) Burns, A. B.; Register, R. A. Thermoplastic Elastomers via Combined Crystallization and Vitrification from Homogeneous Melts. *Macromolecules* **2016**, *49* (1), 269–279.
- (22) Bishop, J. P.; Register, R. A. Thermoplastic Elastomers with Composite
   Crystalline–Glassy Hard Domains and Single-Phase Melts. *Macromolecules* 2010, 43
   (11), 4954–4960.
- (23) Panthani, T. R.; Bates, F. S. Crystallization and Mechanical Properties of Poly(L-Lactide)-Based Rubbery/Semicrystalline Multiblock Copolymers. *Macromolecules* **2015**, *48* (13), 4529–4540.
- (24) Lee, I.; Panthani, T. R.; Bates, F. S. Sustainable Poly(Lactide-b-Butadiene) Multiblock Copolymers with Enhanced Mechanical Properties. *Macromolecules* **2013**, *46* (18), 7387–7398.
- (25) Koo, C. M.; Hillmyer, M. A.; Bates, F. S. Structure and Properties of Semicrystalline-Rubbery Multiblock Copolymers. *Macromolecules* **2006**, *39* (2), 667–677.
- (26) Wang, W.; Lu, W.; Kang, N.-G.; Mays, J.; Hong, K. Thermoplastic Elastomers Based on Block, Graft, and Star Copolymers. In *Elastomers*; InTech, 2017.
- (27) Von Tiedemann, P.; Yan, J.; Barent, R. D.; Spontak, R. J.; Floudas, G.; Frey, H.; Register,
   R. A. Tapered Multiblock Star Copolymers: Synthesis, Selective Hydrogenation, and
   Properties. *Macromolecules* 2020, 53 (11), 4422–4434.

- (28) Shim, J. S.; Kennedy, J. P. Novel Thermoplastic Elastomers. II. Properties of Star-Block Copolymers of PSt-b-PIB Arms Emanating from Cyclosiloxane Cores. *J. Polym. Sci. Part A Polym. Chem.* **1999**, *37* (6), 815–824.
- (29) Bi, L. K.; Fetters, L. J. Synthesis and Properties of Block Copolymers. 3. Polystyrene-Polydiene Star Block Copolymers. *Macromolecules* **1976**, *9* (5), 732–742.
- (30) Nese, A.; Mosnáček, J.; Juhari, A.; Yoon, J. A.; Koynov, K.; Kowalewski, T.; Matyjaszewski, K. Synthesis, Characterization, and Properties of Starlike Poly(n-Butyl Acrylate)-b-Poly(Methyl Methacrylate) Block Copolymers. *Macromolecules* 2010, 43 (3), 1227–1235.
- (31) Burns, A. B.; Register, R. A. Mechanical Properties of Star Block Polymer Thermoplastic Elastomers with Glassy and Crystalline End Blocks. *Macromolecules* **2016**, *49* (24), 9521–9530.
- (32) Juhari, A.; Mosnáček, J.; Yoon, J. A.; Nese, A.; Koynov, K.; Kowalewski, T.; Matyjaszewski, K. Star-like Poly (n-Butyl Acrylate)-b-Poly (α-Methylene-γ-Butyrolactone) Block Copolymers for High Temperature Thermoplastic Elastomers Applications. *Polymer* 2010, 51 (21), 4806–4813.
- (33) Jacob, S.; Majoros, I.; Kennedy, J. P. Novel Thermoplastic Elastomers: Star-Blocks

  Consisting of Eight Poly(Styrene-B-Isobutylene) Arms Radiating From A Calix[8]Arene

  Core. *Rubber Chem. Technol.* **1998**, *71* (4), 708–721.
- (34) Laradji, M.; Shi, A. C.; Noolandi, J.; Desai, R. C. Stability of Ordered Phases in Diblock Copolymer Melts. *Macromolecules* **1997**, *30* (11), 3242–3255.
- (35) Joziasse, C. A. P.; Grablowitz, H.; Pennings, A. J. Star-Shaped Poly[(Trimethylene

- Carbonate)-Co-(ε-Caprolactone)] and Its Block Copolymers with Lactide/Glycolide: Synthesis, Characterization and Properties. *Macromol. Chem. Phys.* **2000**, *201* (1), 107–112.
- (36) Guerin, W.; Helou, M.; Carpentier, J. F.; Slawinski, M.; Brusson, J. M.; Guillaume, S. M. Macromolecular Engineering via Ring-Opening Polymerization (1): L-Lactide/Trimethylene Carbonate Block Copolymers as Thermoplastic Elastomers. *Polym. Chem.* 2013, *4* (4), 1095–1106.
- (37) Kong, J. F.; Lipik, V.; Abadie, M. J. M.; Deen, G. R.; Venkatraman, S. S. Characterization and Degradation of Elastomeric Four-Armed Star Copolymers Based on Caprolactone and L-Lactide. *J. Biomed. Mater. Res. Part A* **2012**, *100 A* (12), 3436–3445.
- (38) Lee, S.; Lee, K.; Jang, J.; Choung, J. S.; Choi, W. J.; Kim, G. J.; Kim, Y. W.; Shin, J. Sustainable Poly(ε-Decalactone)–poly(L-Lactide) Multiarm Star Copolymer Architectures for Thermoplastic Elastomers with Fixed Molar Mass and Block Ratio. *Polymer* **2017**, *112*, 306–317.
- (39) Bucknall, C. B. Toughened Plastics, 1st ed.; Springer Netherlands: Dordrecht, 1977.
- (40) Kong, J. F.; Lipik, V.; Abadie, M. J.; Deen, G. R.; Venkatraman, S. S. Biodegradable Elastomers Based on ABA Triblocks: Influence of End-Block Crystallinity on Elastomeric Character. *Polym. Int.* **2012**, *61* (1), 43–50.
- (41) Matsen, M. W. Effect of Architecture on the Phase Behavior of AB-Type Block Copolymer Melts. *Macromolecules* **2012**, *45* (4), 2161–2165.
- (42) Batiste, D. C.; Meyersohn, M. S.; Watts, A.; Hillmyer, M. A. Efficient Polymerization of Methyl-ε-Caprolactone Mixtures to Access Sustainable Aliphatic Polyesters.

- Macromolecules 2020, 53 (5), 1795–1808.
- (43) Martello, M. T.; Burns, A.; Hillmyer, M. Bulk Ring-Opening Transesterification Polymerization of the Renewable δ-Decalactone Using an Organocatalyst. *ACS Macro Lett.* **2012**, *I* (1), 131–135.
- (44) Lohmeijer, B. G. G.; Pratt, R. C.; Leibfarth, F.; Logan, J. W.; Long, D. A.; Dove, A. P.; Nederberg, F.; Choi, J.; Wade, C.; Waymouth, R. M.; et al. Guanidine and Amidine Organocatalysts for Ring-Opening Polymerization of Cyclic Esters. *Macromolecules* **2006**, *39* (25), 8574–8583.
- (45) Kricheldorf, H. R.; Kreiser-Saunders, I.; Stricker, A. Polylactones 48. SnOct2-Initiated Polymerizations of Lactide: A Mechanistic Study. *Macromolecules* **2000**, *33* (3), 702–709.
- (46) Dria, R. D.; Goudy, B. A.; Moga, K. A.; Corbin, P. S. Synthesis and Characterization of Multi-Armed Calixarene- and Resorcinarene-Core Polylactide Star Polymers. *Polym. Chem.* 2012, 3 (8), 2070–2081.
- (47) Dechy-Cabaret, O.; Martin-Vaca, B.; Bourissou, D. Controlled Ring-Opening Polymerization of Lactide and Glycolide. *Chem. Rev.* **2004**, *104* (12), 6147–6176.
- (48) Brown, H. A.; De Crisci, A. G.; Hedrick, J. L.; Waymouth, R. M. Amidine-Mediated Zwitterionic Polymerization of Lactide. *ACS Macro Lett.* **2012**, *1* (9), 1113–1115.
- (49) Fetters, L. J.; Meyer, B. H.; McIntyre, D. The Effect of Diblock and Homopolymer Impurities on the Morphology of Triblock Polymers. *J. Appl. Polym. Sci.* 1972, 16 (8), 2079–2089.
- (50) Rosenbloom, S. I.; Gentekos, D. T.; Silberstein, M. N.; Fors, B. P. Tailor-Made

- Thermoplastic Elastomers: Customisable Materials: Via Modulation of Molecular Weight Distributions. *Chem. Sci.* **2020**, *11* (5), 1361–1367.
- (51) Smith, T. L.; Dickie, R. A. Viscoelastic and Ultimate Tensile Properties of Styrene-Butadiene-Styrene Block Copolymers. *J. Polym. Sci. Part C Polym. Symp.* **1969**, *26* (1), 163–187.
- (52) Nandan, B.; Hsu, J. Y.; Chen, H. L. Crystallization Behavior of Crystalline-Amorphous Diblock Copolymers Consisting of a Rubbery Amorphous Block. *Polym. Rev.* 2006, 46 (2), 143–172.
- (53) He, W. N.; Xu, J. T. Crystallization Assisted Self-Assembly of Semicrystalline Block Copolymers. *Prog. Polym. Sci.* 2012, 37 (10), 1350–1400.
- (54) Loo, Y. L.; Register, R. A.; Ryan, A. J. Modes of Crystallization in Block Copolymer Microdomains: Breakout, Templated, and Confined. *Macromolecules* **2002**, *35* (6), 2365–2374.
- (55) Price, C.; Watson, A. G.; Chow, M. T. An Investigation of the Effect of Chain Geometry on the Two-Phase Morphology of Polystyrene/Polyisoprene Block Copolymers. *Polymer* **1972**, *13* (7), 333–336.
- (56) Alward, D. B.; Kinning, D. J.; Thomas, E. L.; Fetters, L. J. Effect of Arm Number and Arm Molecular Weight on the Solid-State Morphology of Poly(Styrene-Isoprene) Star Block Copolymers. *Macromolecules* **1986**, *19* (1), 215–224.
- (57) de la Cruz, M. O.; Sanchez, I. C. Theory of Microphase Separation in Graft and Star Copolymers. *Macromolecules* **1986**, *19* (10), 2501–2508.
- (58) Lynd, N. A.; Oyerokun, F. T.; O'Donoghue, D. L.; Handlin, D. L.; Fredrickson, G. H.

- Design of Soft and Strong Thermoplastic Elastomers Based on Nonlinear Block Copolymer Architectures Using Self-Consistent-Field Theory. *Macromolecules* **2010**, *43* (7), 3479–3486.
- (59) Parker, A. J.; Rottler, J. Entropic Network Model for Star Block Copolymer Thermoplastic Elastomers. *Macromolecules* **2018**, *51* (23), 10021–10027.
- (60) Spencer, R. K. W. W.; Matsen, M. W. Domain Bridging in Thermoplastic Elastomers of Star Block Copolymer. *Macromolecules* **2017**, *50* (4), 1681–1687.
- (61) Bernaerts, K. V.; Du Prez, F. E. Dual/Heterofunctional Initiators for the Combination of Mechanistically Distinct Polymerization Techniques. *Prog. Polym. Sci.* **2006**, *31* (8), 671–722.
- (62) Matsen, M. W.; Schick, M.; Mateen, M. W.; Schick, M. Microphase Separation in Starblock Copolymer Melts. *Macromolecules* **1994**, *27* (23), 6761–6767.
- (63) Parker, A. J.; Rottler, J. Molecular Mechanisms of Plastic Deformation in Sphere-Forming Thermoplastic Elastomers. *Macromolecules* **2015**, *48* (22), 8253–8261.
- (64) Ren, J. M.; McKenzie, T. G.; Fu, Q.; Wong, E. H. H.; Xu, J.; An, Z.; Shanmugam, S.;
  Davis, T. P.; Boyer, C.; Qiao, G. G. Star Polymers. *Chem. Rev.* 2016, 116 (12), 6743–6836.
- (65) Milner, S. T.; McLeish, T. C. B. Parameter-Free Theory for Stress Relaxation in Star Polymer Melts. *Macromolecules* **1997**, *30* (7), 2159–2166.
- Johnson, K. J.; Glynos, E.; Sakellariou, G.; Green, P. Dynamics of Star-Shaped
   Polystyrene Molecules: From Arm Retraction to Cooperativity. *Macromolecules* 2016, 49
   (15), 5669–5676.

- (67) Fetters, L. J. L. J.; Kiss, A. D.; Pearson, D. S.; Quack, G. F.; Vitus, F. J. Rheological Behavior of Star-Shaped Polymers. *Macromolecules* **1993**, *26* (4), 647–654.
- (68) Doi, M.; Kuzuu, N. Y. Rheology of Star Polymers in Concentrated Solutions and Melts. *J. Polym. Sci. Polym. Lett. Ed.* **1980**, *18* (12), 775–780.
- (69) Graessley, W. W.; Roovers, J. Melt Rheology of Four-Arm and Six-Arm Star Polystyrenes. *Macromolecules* **1979**, *12* (5), 959–965.
- (70) Ball, R. C.; McLeish, T. C. B. Dynamic Dilution and the Viscosity of Star Polymer Melts. *Macromolecules* **1989**, *22* (4), 1911–1913.
- (71) Pearson, D. S.; Helfand, E. Viscoelastic Properties of Star-Shaped Polymers. *Macromolecules* **1984**, *17* (4), 888–895.
- (72) Shieh, Y. T.; Liu, G. L. Temperature-Modulated Differential Scanning Calorimetry

  Studies on the Origin of Double Melting Peaks in Isothermally Melt-Crystallized Poly(L-Lactic Acid). *J. Polym. Sci. Part B Polym. Phys.* **2007**, *45* (4), 466–474.
- (73) Bates, F. S.; Fredrickson, G. H. Block Copolymer Thermodynamics: Theory and Experiment. *Annu. Rev. Phys. Chem.* **1990**, *41* (1), 525–557.